Multilayer adsorption of xenon, krypton, and argon on graphite: An ellipsometric study

H. S. Youn,* X. F. Meng,† and G. B. Hess
Department of Physics, University of Virginia, Charlottesville, Virginia 22901
(Received 17 May 1993; revised manuscript received 30 July 1993)

We present ellipsometric measurements of multilayer adsorption of xenon, krypton, and argon on highly oriented pyrolytic graphite along numerous isotherms spanning the coverage range from completion of the first layer to about twelve layers and the temperature range from below the melting of the top layer to above the bulk adsorbate melting point T_m. The three adsorbates have very similar phase diagrams, and all show reentrant first-order layering. The top layer of three-layer and thicker films disorders at $0.81T_m$–$0.83T_m$. For films thicker than three layers, first-order layer condensation reappears at shifted coverages and chemical potentials in the range $0.83T_m$–$0.87T_m$ to $0.92T_m$–$0.94T_m$. The solid adsorbate films reach a limiting thickness of about 12 layers at saturation, but the limiting thickness increases rapidly just below T_m and reaches the equivalent of about 24 layers in the liquid region. We discuss implications of these results for roughening and melting of the adsorbate (111) surfaces. Chemical potentials for layer condensation are compared to a simple Frankel-Halsey-Hill theory.

I. INTRODUCTION

More than 20 years ago, Thomy and Duval[1] showed that certain adsorbate films on graphite, including solid krypton and xenon, grow layer by layer to substantial thickness in equilibrium with the vapor. They were able to do this because they prepared exfoliated graphite substrates of sufficient surface homogeneity that volumetric adsorption isotherms showed sharp layer-condensation steps through the fifth layer. This work and subsequent extensions raise a number of issues which have been of interest in the recent years.

One is the question of wetting, particularly by solid films.[2] An adsorbate is said to wet a uniform substrate if it forms a film whose thickness increases uniformly with increasing pressure and diverges as the saturated vapor pressure is approached. Many solid films do not grow beyond one or two layers because of structural incompatibility with the bulk solid phase. In cases where thick films are seen, the question remains whether wetting is complete, or whether, at some finite thickness, strain effects limit uniform film growth in favor of crystallites with minimal connection to the surface.[3]

If thick solid films do occur, then one has the opportunity to study the facet of the bulk crystal which corresponds to the free surface of the film, subject to the perturbation caused by the nearby film-substrate interface. This can be useful to obtain a large specific surface area, in which case the perturbation by the substrate is often a minor inconvenience. However, in thermodynamic measurements this perturbation can be a useful probe, labeling successive layers by shifting them in chemical potential.

One of the properties which has been studied in this way is surface melting.[4] Here the availability of a large surface area allows the application of techniques which are not intrinsically surface sensitive, such as heat capacity,[5] neutron diffraction,[6] and quasielastic neutron scattering (QENS).[7] Another property is surface roughening.[8] Above the roughening temperature of a particular crystal face, steps will proliferate, and that facet will not appear on the equilibrium crystal. This can be studied by direct observation of small crystallites,[9,10] but film experiments give additional information, essentially through the response of the surface to the substrate as a function of thickness.

Following the volumetric isotherm studies of Thomy and Duval, a number of other experiments have confirmed that rare gases form thick films on graphite, and have provided information on their structure. Transmission electron microscope work at Sussex[11] showed epitaxial growth of Xe, Kr, and Ar on clean graphite, with films ranging from 25 to 500 Å in the case of Xe. In these experiments it was not possible to distinguish between equilibrium wetting and uniform growth from supersaturated vapor. Reflection high-energy electron-diffraction (RHEED) studies at Marseille[12,3] showed uniform growth at low temperatures of films of Ar, Kr, and Xe to thicknesses of at least ten layers. These films were grown by dosing at low temperature rather than in equilibrium with the vapor, so again are not sufficient to prove wetting (in the sense defined above).

Zhu and Dash (ZD) (Ref. 5) made heat-capacity studies of argon and neon films adsorbed on exfoliated graphite foam, for a number of adsorbate doses up to the equivalent of more than ten uniform layers. Features were identified with disordering of the top layer at layer critical points (near 68 K, for the third and higher layers of Ar) and melting of each of the bottom four layers. Subsequent work has led to a better understanding of the extent of capillary condensation on this sort of substrate, and required revision of some of the original interpretation.[13,14] In particular, at higher doses a significant fraction of the adsorbate goes into capillary condensation, and the maximum coverage in the uniform part of the

film probably did not exceed five or six layers.

We previously reported results of an ellipsometric isotherm study of argon adsorption on highly oriented pyrolytic graphite (HOPG).[15,16] In agreement with ZD, we found layer critical temperatures near 68 K, above which the layer-condensation steps started to become broad. However, it was found that sharp steps reappeared at temperatures a few degrees higher, corresponding to a new region of apparent first-order condensation, for the fourth and higher layers. These sharp steps persisted up to about 77 K, then again became broad. This result raises several questions: Which sequence of critical points is related (see below) to the roughening temperature of Ar(111), those near 68 K or those near 77 K? What mechanism produces first-order layer-condensation transitions rather than continuous growth after the top layer of the film is apparently disordered? How does the film melt, and how do layer melting transitions relate to the layer critical points? What is the evidence for surface melting Ar(111)? Is this reentrant first-order behavior unique to argon, or is it common to other adsorbates?

In this paper we present the argon results in greater detail, in addition to reporting extensive ellipsometric isotherm studies of xenon and krypton films on HOPG. One principal conclusion is that these three adsorbates show great similarity in the multilayer regime, beyond the first layer, with layer critical points and reentrant first-order regions at nearly the same reduced temperatures, when scaled by the bulk melting temperature.

The paper is organized as follows: Section II summarizes certain points of the theoretical background. Section III gives a description of the experimental technique. In Sec. IV we briefly review earlier work and present our results for xenon, krypton, and argon. The results are discussed and compared to other recent work in Sec. V.

II. THEORY

A. Wetting, surface melting, surface roughening, and preroughening

A simple liquid adsorbate is expected to wet any substrate to which it is more strongly attracted than to its own bulk liquid phase. If the substrate attraction is weaker, so that it does not wet, the adsorbate beyond some thickness will bead up into droplets. In the case of a solid adsorbate film there are additional constraints which may prevent wetting: If the structure of the first layer or two of the film on the substrate does not match the structure of any plane of the bulk solid, then there will be a free-energy barrier which is likely to prevent further growth. This is not likely to be a problem with spherical molecules. Even if there is no structural incompatibility, the stronger attraction of the substrate will in general compress the film laterally relative to the corresponding plane of the bulk solid, at least at $T=0$.[3] As the film grows, provided its layers remain mutually commensurate, the lateral compressive stress will be distributed over the whole thickness d of the film, and the strain will decrease as $1/d$. The increment of strain energy with coverage then will fall off as d^2, which is less rapid than the decrease of the van der Waals potential; therefore the uniform film will eventually become energetically unfavorable relative to a free three-dimensional crystal. Model calculations by Gittes and Schick[17] yield a limiting thickness exceeding 20 layers for Xe, Kr, and Ar, and increasing rapidly in that order as the (predicted) dilation[18] of the monolayer with respect to the bulk decreases. The numbers are sensitive to model parameters, but show that substantial differences should be expected for different adsorbates. The case where the thickness of the solid film is limited by strain energy may lead to one form of triple-point wetting: If surface melting also occurs, then the quasiliquid layer (see below) does not support shear stress, and the total film thickness may increase on approaching the bulk melting point from below.

Dash[19] has proposed a different mechanism by which substrate heterogeneity may limit solid film growth. He suggests that differently oriented film grains will grow over different substrate grains or patches, and the boundaries separating these film grains must grow through each added layer. This contributes a fixed energy cost for each added solid layer, determined by the substrate grain size, which will eventually exceed the substrate van der Waals potential energy of the layer and prevent further uniform growth.

Thick films can be used to study the question of surface melting at the face of the bulk crystal which corresponds to the free surface of the film.[4,2] Surface melting means a layer at the surface melts (i.e., becomes disordered and mobile) below the bulk melting temperature of the crystal, and the thickness of this "quasiliquid" layer diverges as the bulk melting temperature is approached. In a finite film this process cannot go to completion. In addition the lower layers approaching the substrate may be stabilized progressively against melting; indeed, a converse effect of substrate-induced freezing may occur at the lower interface.[20] But sufficiently thick films should provide an adequate surrogate for the bulk surface.

If thick films occur, then one can also ask whether the film grows continuously or stepwise, by successive first-order condensation of dense layers. The sequence of layer critical temperatures $T_{c,n}$ which separates these regimes is predicted to approach the bulk roughening temperature T_R, so that layer-by-layer growth corresponds asymptotically to a smooth facet, and continuous growth to a rough surface.[21] This connection is intuitive if one supposes the layer-condensation transition corresponds to adding one more layer on top of a nearly passive initial film: If the free energy required to add a length of step in the partially filled top layer is positive, then the layer is below its critical temperature and also the bulk surface is smooth. The actual situation may be more complicated, as we shall see below. If there is an attractive interaction preferentially between steps of opposite orientation, this may lead to *preroughening* of the bulk surface: There then may be a temperature range in which steps proliferate, but are correlated in up-down sequence, so that net offsets greater than one layer do not proliferate.[22] This is the disordered-flat phase.

Some insight into the nature of the roughening transi-

tion can be gained from Monte Carlo simulations of a simple lattice-gas mode,[8] which treats a solid terminating with a filled layer at low temperatures. As the temperature is increased toward the roughening temperature T_R, adatoms and vacancies proliferate and cluster into islands and wells, which gain their own islands and wells as the characteristic lateral scale diverges. This cascade process is supposed to unlock the roughened surface from the initial lattice plane. Consistent with the divergence of the lateral correlation length at a Koterlitz-Thouless transition, on the local scale sampled by the simulation there is no sharp signature of the roughening transition.

Of more direct applicability to the present experiments are several simulations of the (111) surface of a fcc Lennard-Jones solid.[23] These show disordering of the top layer at a temperature near $0.8T_m$, with adatom promotion (vacancy formation) precursive to the loss of in-layer structure and the appearance of large transverse mobility. A similar disordering of the second-to-top layer occurs near $0.9T_m$. While the small scale of simulations precludes a direct identification of the roughening transition, it would be expected to occur in the region of top-layer disordering, as that is an indication of step proliferation. At the same time, the mobility increase indicates that the first layer goes to a "quasiliquid" state, as do the next two layers at somewhat higher temperatures. If this continues to diverging depth as T_m is approached, then surface melting is occurring. Thus an intuitive picture is supported in which disordering of the top layer is both an immediate precursor of surface roughening, and also the first step of surface melting if that occurs.

The surface of a finite film, if the film has the same structure as the corresponding bulk phase, may nevertheless differ from the bulk surface in several ways. The phonon spectrum is modified, especially for very thin films, and this generally lowers the critical temperature of the monolayer. In thicker films, the bottom few layers may remain solid above the bulk melting point due to compression, and the rigid boundary may induce layering in liquid films to considerable thickness.[24] The chemical potential will be shifted by the substrate potential, as discussed below, and this will couple to transitions involving changes in density.

B. Substrate potential and layer chemical potentials

The long-range, laterally averaged, attractive potential of a substrate for a molecule at distance z from the surface has the van der Waals form

$$V(z)=-\frac{C_3}{(z-z_0)^3} \tag{1}$$

when retardation is neglected.[25] Here the substrate has been replaced by a semi-infinite continuum, and z_0 is the edge of the continuum (image plane), relative to the central plane of the top layer of atoms (see Fig. 1). In addition there should be terms representing short-range repulsion, lateral modulation with the periodicity of the substrate structure, and shorter-range attractive terms. We are interested in the thermodynamic properties of a condensed film in the presence of this potential. In the

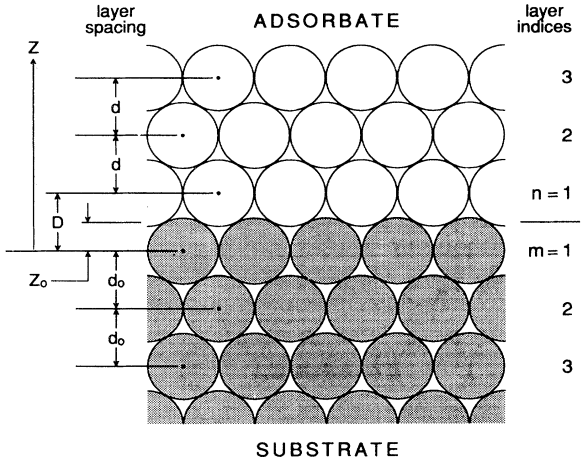

FIG. 1. Schematic representation of layers of substrate atoms (shaded circles) and adsorbate atoms (open circles). In the model leading to Eq. (1), the substrate is replaced by a dielectric continuum filling the half-space below $z=z_0$. In Eq. (2) it is assumed that $D=(d_0+d)/2$, while Eq. (3) is written for $D=d$.

event that the structure of a multilayer film is very similar to the structure of a bulk phase of the adsorbate, the Frankel-Halsey-Hill (FHH) model provides a useful simple approximation.[26] In this approximation the film is treated as a slab of the appropriate bulk phase placed in the potential of the substrate, so that the interaction energy is obtained by simply adding up the potential energies of the adsorbate atoms at their specified locations. This model can be refined by introducing interfacial energies or by allowing elastic relaxation of the film,[27] but only the simplest model will be employed here. The chemical potential is the energy required to add one molecule at the free surface of the film, which is at a height z above the substrate, so $\mu(z)=\mu_0+V(z)$, where $\mu_0(T)$ is the chemical potential of the bulk phase in coexistence with vapor. In evaluating film chemical potentials, a semi-infinite slab of bulk adsorbate is used as a reference, so that the effective potential associated with the difference is the potential of the substrate, less the potential of the continued adsorbate which replaces it in the reference state. Thus, for example, for argon adsorbed on graphite, the effective C_3 in Eq. (1) is the value for Ar/graphite (1210 meV Å^3) less the value for Ar/Ar (506 meV Å^3)[25]. We are interested in evaluating the chemical potential μ_n at the layering transition at which an n-layer film coexists with an $(n-1)$-layer film; thus a molecule is being added to the nth layer. In the spirit of the FHH model, the lower $n-1$ layers are supposed to be passive on addition of the nth layer (or at least the surface is translated upward invariantly, except for the reduction in substrate potential.) Then

$$\mu_n-\mu_0=V_n=-(C_3/d^3)(n-\tfrac{1}{2})^{-3}\ , \tag{2}$$

which is Eq. (1) with $z=(d_0+d)/2+(n-1)d$ and $z_0=d_0/2$, where d is the adsorbate-layer spacing and d_0 is the graphite-layer spacing. Since the surface of the continuum representing the graphite is $d_0/2$ above the

plane of the top-layer carbon nuclei, this choice of z_0 corresponds to a spacing between the planes of the top layer of substrate atoms and the first layer of adsorbate atoms equal to $(d+d_0)/2$, as is illustrated in Fig. 1.

If the substrate is graphite, on account of the layer structure one might hope to improve on the approximation of Eq. (2) by smoothing only over layers, and summing the contributions of the layers.[28] This gives

$$\mu_n-\mu_0=V_n=-(C_3/d^3)(3d_0/d)\sum_{m=0}^{\infty}[n+m(d_0/d)]^{-4}\ . \tag{3}$$

However, this form is not quite so appropriate for the reference state, and may overcorrect the difference. An expansion of Eq. (3) yields Eq. (2) with $[n-1/2-O(1/n)]$ replacing $(n-\frac{1}{2})$.[28]

C. Thermodynamic relations

Experimentally, the chemical potential of the film is determined using the ideal gas relation for the coexisting vapor,

$$\mu-\mu_0=k_BT\ln(p/p_0)\ , \tag{4}$$

where p_0 is the vapor pressure of the bulk adsorbate at the same temperature. Henceforth we will measure chemical potential in temperature units, so that $k_B=1$.

The slope of a line of constant coverage in the $\mu-T$ plane is related to the partial entropy by the Maxwell relation

$$\left[\frac{\partial\mu}{\partial T}\right]_N=-\left[\frac{\partial S}{\partial N}\right]_T\ . \tag{5}$$

This can be applied to a layer-coexistence line (which includes a finite range of coverages), or to the bulk phase, in which case the partial entropy is the bulk molar entropy. If a system is accurately described by the FHH model, then the partial entropy of the film should be equal to the bulk molar entropy, so the layer condensation line $\mu_n(T)$ must be parallel to the bulk saturation line $\mu_0(T)$. We will find that this is reasonably well satisfied for higher layers, and take this as partial justification for applying Eqs. (2) or (3) to extract information about the adsorption potential.

A critical point terminating a first-order phase transition between two two-dimensional (2D) phases of the same symmetry, e.g., 2D liquid-vapor coexistence on top of an inert underlayer, should belong to the universality class of the 2D Ising model. Therefore various properties should obey known scaling laws in the vicinity of the critical point; in particular, the compressibility along the critical isochore above the critical temperature T_c should vary as $(T-T_c)^{-\gamma}$, with $\gamma=\frac{7}{4}$. We will assume this dependence in analyzing data, but in some cases it is possible that there might be an additional first- or second-order phase-transition line present, in which case the presumed critical point might actually be a triple or tricritical point.

III. EXPERIMENTAL PROCEDURE

A. Cryostat

We chose to locate our adsorption cell within a cryostat, so that the cold walls of the cell would protect the sample from contamination resulting from outgassing. This has proved very effective, as we are able to conduct runs of two months duration with no indication of any changes due to contaminants. This entails certain limitations compared to the alternative approach of placing the sample on a cold finger in a mostly room-temperature UHV chamber, to which the adsorbate is admitted. Most facilities for sample cleaning and characterization, such as ion etching and low-energy electron diffraction (LEED), cannot be used, and the mechanical connection between the sample and the ellipsometer is not as rigid.

The graphite sample is located in an ion-pumped stainless-steel cell near the bottom of the cryostat vacuum jacket, which contains window ports. The cell consists of three 18-mm-i.d. tees joined by copper-gasketed miniflanges, and connected by a vertical 31-mm-i.d. stainless-steel tube to the ion-pump manifold above the cryostat. The graphite sample is clamped to a copper finger, which enters the cell through one port of the lowest tee. The surface of the graphite can be observed at an angle of incidence of 45° through a glass window sealed to the sidearm of the tee. The optical configuration is described below. Another port contains a second cold finger, which is used to control the adsorbate pressure. The cell, sample mount, and cold finger are connected by separate copper braids to a thermal platform, which is cooled by the second stage of a closed-cycle refrigerator[29] and is electronically regulated to a temperature suitably below the desired sample temperature. The sample mount is temperature regulated by a second ac bridge, using a platinum film thermometer and a heater attached to the end of the sample mount finger, where it joins the cooling braid. A separate platinum thermometer slightly closer to the sample is employed to monitor the temperature of the sample mount, and an oxygen vapor pressure bulb is available for calibration. Manually adjusted heaters control the temperatures of the body of the cell and the cold finger. The cell is normally maintained a few degrees warmer than the sample, as it is desired that the sample be the coldest surface exposed to the adsorbate gas. To approach this objective, the sample mount finger is sealed to the cell via a reentrant stainless-steel tube which extends to within a few mm of the sample. The sample is covered by a copper cap, except for a 6-mm-diam hole in line with the window. This cap is intended to intercept heat conducted through the gas from the warmer cell walls, so as to provide a nearly isothermal environment for the sample. We believe, for reasons discussed in Sec. V D, that this reduces to a few mK the temperature difference between the graphite surface and the coldest spot exposed to the vapor. The cap also supports a mirror used in the return-path ellipsometric configuration.

The pressure in the cell is measured by three capacitance diaphragm gauges at room temperature, with ranges of 10, 100, and 1000 Torr.[30] For some earlier runs

the 100-Torr gauge was not yet installed. A zero-offset correction was applied to the 10-Torr gauge readings, based on the recorded output while under vacuum at the start of the run. Zero corrections to the other gauges were based on comparison with the next more sensitive gauge in the pressure region of overlap.

It is convenient to use the platinum resistance thermometer on the sample mount (1000 Ω film type) with a nominal calibration to provide a working temperature scale. However, this scale can be in error by as much as 2 K. For final temperature estimates, we use the saturated vapor pressure of the adsorbate as determined in the course of the isotherm, together with a polynomial fit to saturated vapor pressure data from the literature.[31] We believe that this temperature scale is accurate to within 0.2 K over the range of each of the three gases. Over the course of an isotherm, the sample temperature is regulated to a precision of about ±10 mK, except when, at saturation, bulk adsorbate is being condensed or evaporated.

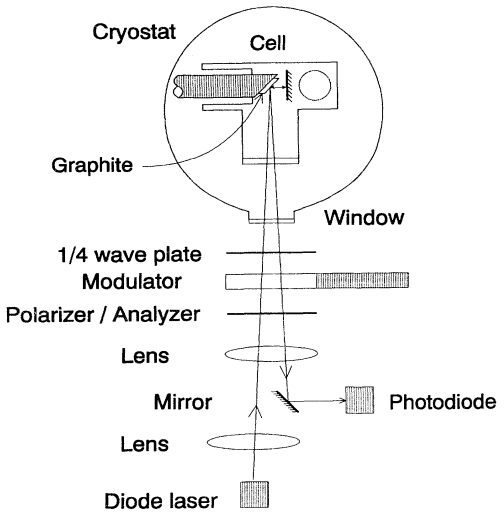

FIG. 2. Schematic diagram of the cell and optical setup, which is configured as a return-path phase-modulated ellipsometer.

B. Ellipsometry

We monitor the coverage of adsorbate on the graphite substrate by an ellipsometric technique. Reflectance ellipsometry measures the ratio ρ of the reflection coefficients for *p*- and *s*-polarized light, and the relative phase delay Δ between the two polarizations. If a transparent film is deposited on a reflecting surface, the principal effect is to increase the relative phase delay Δ by an amount proportional to the film thickness, provided the film is very thin compared to the wavelength of the light. We wish to arrange the optical system to provide an output proportional to $\Delta-\Delta_0$, where Δ_0 is the delay for the bare substrate. A simple arrangement for this purpose was described previously.[32] Light from a diode laser which is linearly polarized at an angle of 45° to the plane of incidence passes through a phase-delay modulator and reflects from the sample at an angle of incidence of 45°. The reflected light passes through a $\frac{1}{4}$-wave plate and an analyzer oriented at 45° to the plane of incidence, then to a photocell. The modulator is a rectangular prism of fused silica, driven at its extensional resonance, which adds a 50-Khz ac phase delay to Δ.[33] The output of interest (I_1) is the Fourier component of the photocurrent at the modulation frequency. It was shown that this is proportional to a linear combination of $\rho\sin(\Delta)$ and $\rho\cos(\Delta)$, with coefficients dependent on the orientation angle α of the $\frac{1}{4}$-wave plate. The angle α can be chosen to null I_1 for the bare substrate; then, when a film is deposited, I_1 will be proportional to $\rho\sin(\Delta-\Delta_0)$. The present experiments used a slightly different optical configuration shown in Fig. 2. The light (at $\lambda=750$ nm) makes two reflections from the sample, passes twice through the $\frac{1}{4}$-wave plate and modulator, and the same calcite prism serves as polarizer and analyzer. The analysis is more complicated,[34] but for practical purposes the dependence of I_1 on film thickness is essentially the same. This configuration requires only one window in the cell, and appears to have some advantage in mechanical stability. The laser power entering the cryostat is about 1 mW. It was verified that this does not produce significant heating of the sample.

C. Procedure

The sample is a rectangular slab about $5\times10\times0.3$ mm^3, cut from the same parent HOPG specimen as the substrates used in our earlier experiments. This sample was installed in October 1988. It was cleaved in air with adhesive tape, baked in flowing argon at 500 °C, and clamped to the copper sample mount in air. The cell and UHV system had been baked previously, and were backfilled with dry nitrogen during this operation. The sample mount assembly was then reinstalled in the cell and evacuated by sorption and ion pumps. When the base pressure had been reached, and shortly before the cryostat was assembled and cooled, the sample mount was heated to 300 °C overnight. The base pressure near the ion pump is on the order of 10^{-8} Torr or less. A residual gas analyzer near the ion pump shows typical outgassing products, including hydrogen, CO, CO_2, methane, and water, as well as helium. Before the experiments described here, several runs with oxygen were carried out, followed by argon, methane, krypton, xenon, nitrogen, and fluoroform; then xenon and krypton were repeated. After each run the remaining adsorbate gas was evacuated and the cell was left open to the ion pump. Preceding each run the sample heating procedure was repeated. No change in rare-gas adsorption isotherms was detected either in the course of a run or between runs. We believe that this observation, together with the sharpness of layer-condensation features and the agreement of layer-condensation chemical potentials with values reported by other laboratories, constitutes strong evidence against the occurrence of significant contamination.

During the cooldown, the sample mount is heated at a low power, so that it remains several degrees warmer than the cold finger. This is intended to discourage the condensation of residual gas on the sample; we do not know that it is necessary. When the operating temperature is reached, the sample temperature regulator is turned on and the temperature of other components of the system including the cold finger are manually adjusted to be slightly warmer than the sample. At this point the ion-pump valve is closed, and a leak valve from the gas handling system is opened to admit adsorbate at an appropriate rate to begin the first isotherm.

An IBM-XT-compatible computer with 12-bit analog-to-digital converter (ADC) card records the outputs of the pressure gauges[35] and the ellipsometer at 2-s intervals, together with various auxiliary signals: The sample temperature regulator bridge unbalance, the cold finger heater voltage, and other heater voltages.

The ellipsometer signal is processed as follows before it is recorded: The dc component of the photocurrent (I_0) is extracted by a low-pass filter channel. For thin films and the ellipsometer settings which null I_1, and the usual modulation amplitude, this signal is only weakly dependent on the film thickness. For thicker uniform films, comparable to the wavelength of light, I_0 shows a substantial periodic reduction, which corresponds to interference fringes in the film. This can be useful in characterizing such films. In most isotherms of the present study, when the vapor pressure reaches saturation, three-dimensional crystallites form on the sample, scattering light, and this produces an abrupt decrease in I_0. This is the most useful indication of reaching the saturated vapor pressure. The accuracy of saturated vapor pressure determination by this method is confirmed by quasiequilibrium measurements of pressure when all of the excess adsorbate in the cell is condensed on the sample and sample mount. (Another indication is an increase in the unbalance signal of the sample mount temperature regulator due to heat of condensation; however, because the thermometer is several centimeters from the sample, this appears only after a delay of 5–20 s, depending on the temperature.)

In the ac channel, the total photocurrent is normalized by an analog "automatic gain control" circuit to maintain a constant dc component. The normalized current is processed by a phase-sensitive detector locked to the modulator frequency, to give I_1. A second phase-sensitive detector extracts the Fourier component at twice the modulation frequency (I_2); this contains ellipsometric information complementary to I_1, but is of interest only for thick films, or for characterization of the substrate.

After the vapor pressure reaches saturation in the first isotherm of a run, the leak valve is closed, and the pressure is reduced by allowing the cold finger to cool below the temperature of the sample, and eventually cold enough to draw off all but the first layer of the adsorbate from the sample. On subsequent isotherms, the pressure is controlled by heating the cold finger, and the leak valve is opened only when there is insufficient gas to reach saturation at a higher temperature. When we are not collecting data, the sample temperature is regulated and the cold finger is allowed to cool.

IV. RESULTS

A. Xenon

A number of experiments have shown that xenon forms multilayer solid films on graphite.[1,11,36] Inaba, Morrison, and Telfer[37] reported incomplete wetting below 116.3 K, but subsequent work[38] indicated that they failed to reach saturation. In an x-ray-diffraction study of xenon on single-crystal graphite, Hong and Birgeneau[39] observed tens of layers near 100 K, but incomplete wetting at lower temperatures, with only six layers below 55 K. It seems possible that this could have been caused by a small temperature difference between the sample and the vermicular graphite ballast. The structure of films of several layers is similar to bulk xenon, except that stacking faults are common.[39] In a mass-loading isotherm study of xenon on a vibrating graphite fiber, Zimmerli and Chan[40] found a maximum of four layers at 106 K. The theoretical expectation is that wetting will be not quite complete, due to strain, with a limiting thickness of several tens of layers.[17] Multilayer Xe films also have been studied on platinum (111).[41]

Our main study consists of 123 ellipsometric isotherms spanning the temperature range 123–163 K. A brief report on this work has appeared as part of a review.[42] This was supplemented by a later run of 43 isotherms in the high- and low-temperature regions. An earlier set of isotherms covered the range 71–115 K. In that range the adsorption steps show considerable kinetic broadening, while steps in desorption remains sharper. Chemical potentials for condensation of layers 2, 3, and 4 relative to the bulk are nearly horizontal. Below about 80 K, films grow to thicknesses of several wavelengths of light while remaining relatively uniform, i.e., without strong light scattering. In the present work, below about 133 K, the isotherms exhibit sharp steps (apart from slow kinetics at the lower temperatures), corresponding to first-order layer-condensation transitions. Figure 3(a) shows a hysteresis loop for third-layer condensation at 116.5 K, including several downward scanning curves. This hysteresis is consistent with a first-order transition limited by kinetics of layer nucleation and possibly growth.[43] The width of the absorption branch varies linearly with temperature, extrapolating to zero about 4 K above the critical temperature for each layer above the second. This width may reflect a distribution of step nucleation barriers for film crystallites on substrate crystallites of different lateral sizes. The nucleation barrier derives from the step free energy, which is expected to go to zero at the layer critical temperature.[44] The remaining width at T_c may have a different origin, in substrate heterogeneity.

Above their critical points the steps broaden and hysteresis is no longer observed. Figure 3(b) shows six adsorption isotherms in the neighborhood of the critical temperatures of the low-temperature first-order layering transitions. At 132.5 K all the steps are sufficiently nar-

row that, for the pressure ramp rate used for this isotherm, only an upper limit can be placed on the widths. The second step (near a reduced pressure of 0.51) shows a clear progression in successive isotherms through a critical point near 136 K. The third step begins to broaden near 133 K, and becomes very wide by 145 K. Near 136 K, a small kink develops at a reduced pressure between the third and fourth steps, and on increasing temperature develops into a new sharp step, designated 4′. (This label reflects the fact that the total coverage is already approximately three layers at the base of this feature, but it is distinctly different from the low-temperature fourth step, appearing at a different reduced pressure.) The low-temperature fourth step begins to broaden near 134 K, but its upper half remains moderately steep (e.g., at 135.1 K) and evolves into a sharp step designated 5′ at slightly higher temperatures. A similar evolution occurs in the higher-layer steps, although the maximum width in the transition region decreases with increasing layer number. It is clear that reentrant first-order layering is occurring, very similar to that we previously reported for argon on graphite.[16] The present xenon data have a somewhat better signal-to-noise ratio.

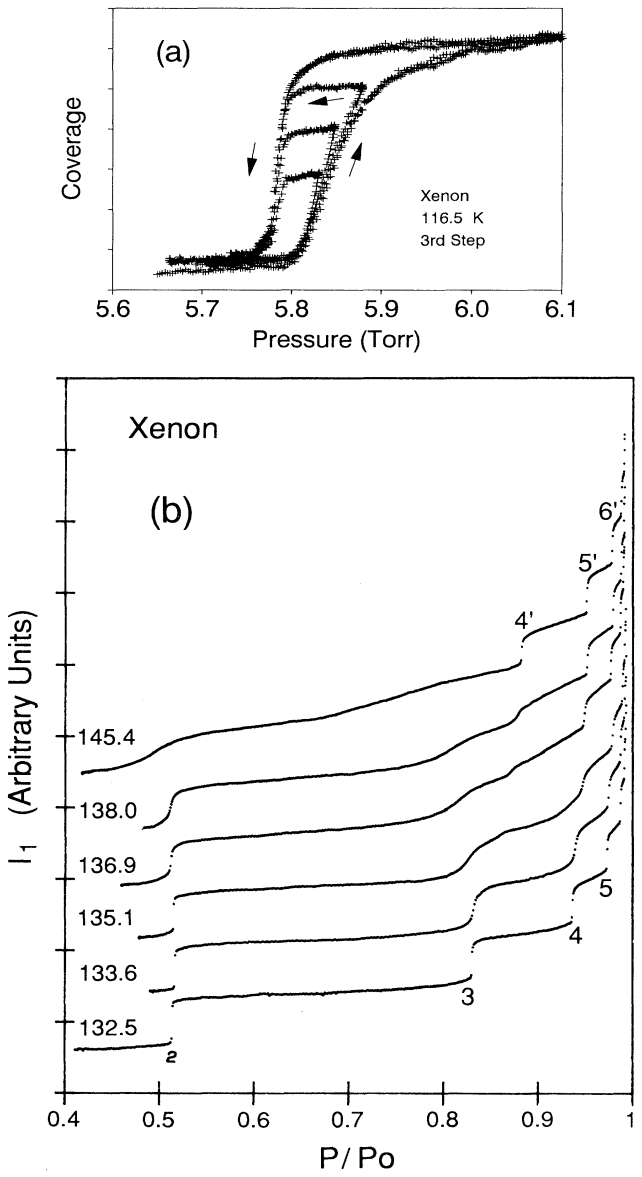

FIG. 3. (a) Hysteresis loop for the third-layer condensation of xenon on graphite at 116.5 K (traversed twice) and three downward scanning curves. The descending branch may be close to equilibrium, while the ascending branch is affected by layer nucleation kinetics. (b) Selected adsorption isotherms for xenon on graphite, shown as ellipsometric coverage vs reduced pressure (p_0=saturated vapor pressure). Temperatures are given at the left.

We have analyzed these isotherms by measuring the pressure and the slope at the inflection point of each step, as well as the relative coverage I_1 at the midpoint of the step. [Below 133 K we take the pressure at the base of the step, because the broadening at low temperature is thought to be kinetic, and the hysteresis is minimum at the base. See Fig. 3(a).] From the pressure p_n at condensation of the nth layer, we calculate the chemical potential μ_n at the coexistence of n and $n-1$ layers, relative to that of bulk solid-vapor coexistence, using Eq. (4). From the slopes we calculate step widths by dividing into a nominal step height, equal to the average coverage per layer for the second, third, and fourth layers at low temperatures. It should be noted that, in the case of a small feature such as the incipient 4′ step, the width so defined is wider than the actual feature, and is more properly regarded as a measure of inverse slope. Both chemical potential and width data are presented in Fig. 4(a) for steps 2 and 3, and in Fig. 4(b) for 3–6′, where the bars represent the widths and the centers of the bars give the chemical potentials as tabulated. The third step is not shown above 137 K in Fig. 4(b). The higher steps are also omitted; we generally resolve up to 7–8′ for $125 < T < 153$ K. Note that the third step moves down with increasing temperature, then levels off at a chemical potential of -53 K and narrows to a width of about 15 K in the temperature range $152 < T < 158$ K. In Fig. 4(c), we show the low-temperature data for third-layer adsorption (crosses and light bars) and desorption (solid circles and heavy bars). Thus the symbols represent chemical potentials measured at the bottoms of the steps. Note that the steps in desorption remain relatively narrow, and have little or no slope in Fig. 4(c).

Step 5′ develops out of the top half of step 4, as is apparent on close examination of Fig. 3(b); thus these steps appear continuous in Fig. 4(b). [Less steep features, such as the lower half of step 4 at 135.1 K, are not represented in Fig. 4(b).] The widths of steps 4′, 4–5′, and 5–6′ are plotted against temperature in Fig. 5. The peak near 135 K, and to a lesser degree the second peak near155 K, decrease rapidly in height with increasing layer number. In the reentrant region of sharp steps centered around 145 K, the steps are approximately as narrow as the corresponding low-temperature steps just below the critical temperature; therefore it seems probable that they represent first-order phase transitions, broadened by substrate heterogeneity. The widths in the first-order regions decrease only slightly with increasing layer number. Dis-

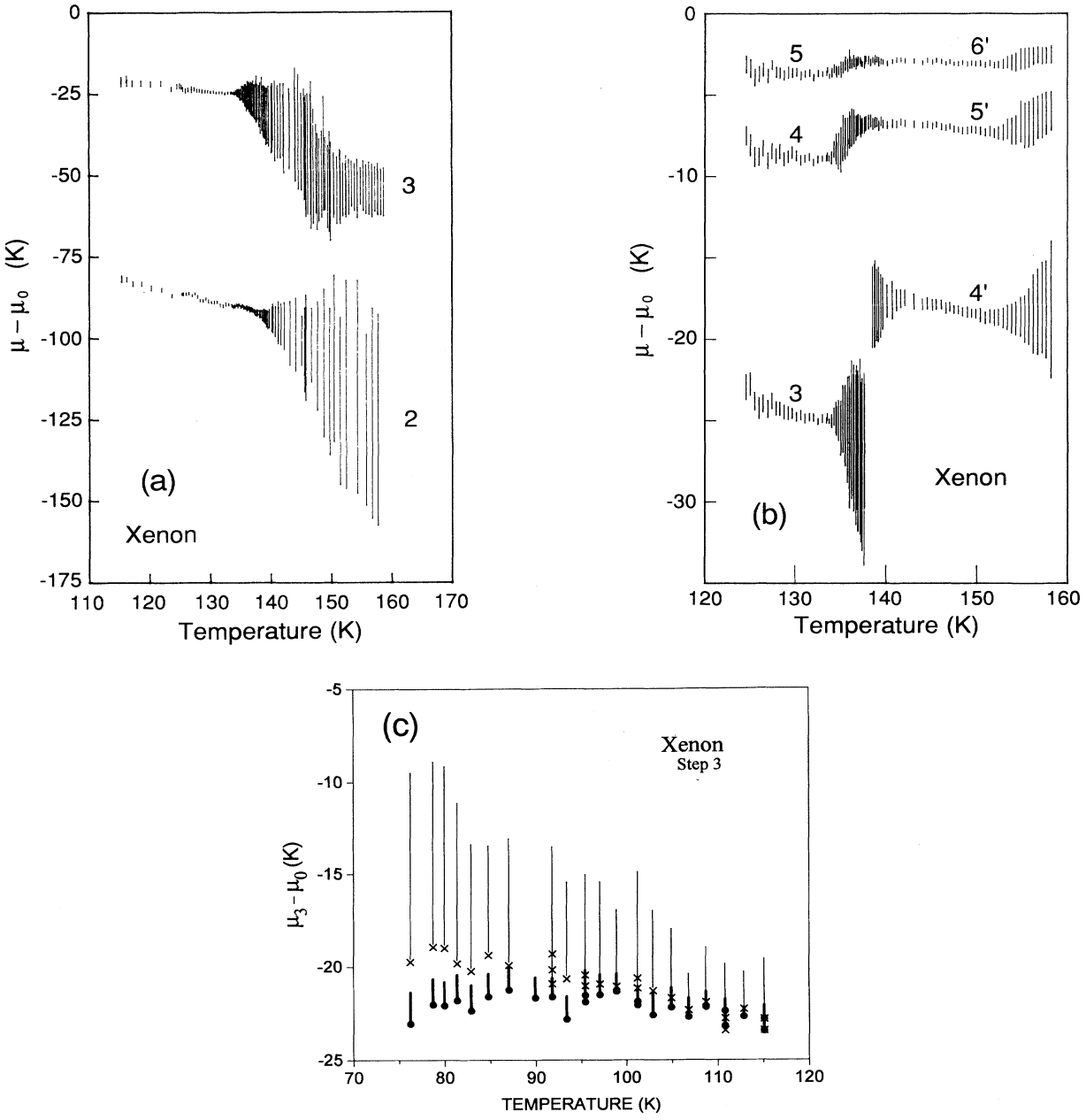

FIG. 4. (a) Xenon-layer-condensation chemical potentials and widths for layers 2 and 3. (b) Layers 3–6′ on an expanded scale. (c) Low-temperature data for third-layer adsorption (crosses and thin bars) and desorption (solid circles and thick bars). μ_0 is the chemical potential of the bulk solid-vapor coexistence.

cussion of the nature of the coexisting phases is deferred to Sec. V.

For each step we have attempted to analyze the width as a function of temperature to obtain the critical temperatures which bound the first-order regions. For layers above the third, there are three such temperatures: $T_{c,n}$ terminating the low-temperature first-order region of step n; and inverse critical point $T_{i,n'}$ and critical point $T_{c,n'}$ bounding the n' reentrant first-order region. A fit is made under the assumption that the slopes of isotherms in the single-phase region near a critical point are described by the 2D Ising compressibility exponent $\gamma = \frac{7}{4}$, and that the background width measured in the two-phase regions adds in quadrature, as would be appropriate for broadening by long-wavelength substrate inhomogeneity.[45] The resulting critical temperatures are given in Table I. Analysis under the assumption that $\gamma = 1$, or assuming the background adds algebraically, would give slightly higher critical temperatures (lower $T_{i,n'}$). The critical temperatures obtained by combining both these assumptions are also given, in brackets, in Table I. Our data are not adequate to fit γ, but a value greater than 1

TABLE I. Xenon-layer critical points, inverse critical points, and second critical points from fits to step widths. The first value is based on the assumptions that $\gamma=\frac{7}{4}$ (Ising critical point) and that the background width adds in quadrature. The value in brackets is based on the assumptions that $\gamma=1$ and that the background width adds algebraically. Mixing these assumptions gives intermediate values. The quoted errors do not include a systematic uncertainty in the temperature scale of up to 0.2 K.

Layer	T_c (K)		Layer	T_i (K)		$T_{c'}$ (K)	
2	136.2(2)	[137.9(3)]					
3	133.5(2)	[134.4(2)]	4′	142.5(3)	[140.6(5)]	151.9(7)	[153.9(4)]
4	133.5(2)	[134.1(1)]	5′	139.9(5)	[138.6(6)]	149.5(6)	[151.7(3)]
5	133.4(3)	[133.8(1)]	6′	139.8(8)	[138.1(3)]	149.9(5)	[151.9(2)]
6		[133.9(4)]	7′				[151.1(6)]

is clearly indicated in many cases. Figure 6 shows the step widths for the second and third layers, raised to the $\frac{4}{7}$th power, which should give a straight line above T_c for an Ising transition. These data are consistent with a straight line over an interval of a few K above T_c.

For comparison with the FHH model, we have averaged the layer-condensation chemical potentials for 13 isotherms in the 6-K interval just below the first critical points, and separately for 16 isotherms in the middle of the reentrant first-order region. These data, together with the residuals of fits by Eq. (3), are given in Table II. For the low-temperature region we obtain $C_3/d^3=440$ or 433. [With Eq. (2), the value obtained for C_3/d^3 is 393 or 403, with comparable residuals.] For the reentrant region a substantially better fit is obtained with a revised model, which assumes the top layer is exactly half-filled before and after each transition; thus the model $\mu_{n'}$ is taken to be $(\mu_n+\mu_{n-1})/2$, where these are given by Eq. (3). This fit gives $C_3/d^3=471$, in reasonable agreement with the low-temperature fit. (Better agreement would be obtained if the fractional filling of the top layer were adjusted from 0.5 to 0.42).

The ellipsometric coverage at the midpoint of the riser of each step is shown in Fig. 7. Since the ellipsometric signal corresponding to the bare graphite is not directly known except in the first isotherm of a run, due to drift or adjustments of the ellipsometer, the midpoint of the second layer is used as the reference. This reference remains well defined above $T_{c,2}$ because the second step remains approximately antisymmetric about its center point. It is apparent that when step 4′ appears, it is located at a coverage midway between the midpoints of low-temperature steps 3 and 4. The loci of the "primed" steps have distinct slope. We do not completely understand this increase in coverage with temperature. The extra coverage is mostly accumulated between the lower

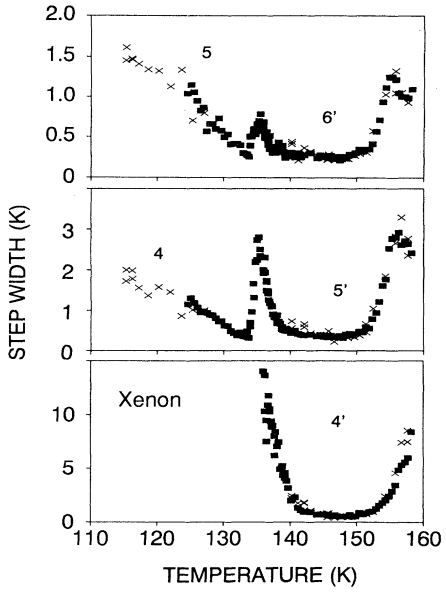

FIG. 5. Widths of several xenon-layer-condensation transitions as functions of temperature. Squares and crosses are data from the first and second runs, respectively. The minimum widths in the reentrant regions 5′ and 6′ are approximately equal to the widths just below the critical points near 133.5 K, and may represent the effect of substrate heterogeneity. The peak near 135 K, attributed to disordering of the top layer, becomes weaker for higher layers.

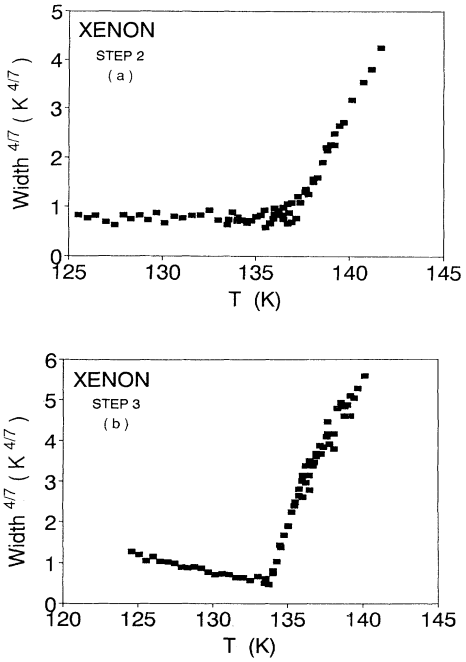

FIG. 6. (a) Width of the second-layer-condensation step to the 4/7th power vs temperature. For an Ising transition, this should yield a straight line in a region above T_c, apart from background subtraction. (b) Same for the third layer.

TABLE II. Layer-condensation chemical potentials and their slopes vs temperature for xenon in a temperature interval below the first critical point, and in the reentrant region (from fits to N isotherms with mean temperature $\bar{T}$). The last two columns give the residuals of fits of Eq. (3) with $d/d_0=1.084$ to the indicated layers, together with the fitting parameters obtained. (Values in parentheses are layers not included in the fit.) The model designated "two layer" assumes that the top layer is exactly half-filled before and after condensation, so that equal numbers of atoms are added to layers $n=n'$ and $n=n'-1$.

Low $T(N=13, \bar{T}=129.7$ K)

			Chemical potential (K)	
Layer	Slope	Measured	Residual (3–7)	Residual (4–7)
2	−0.58(8)	−88.73(43)	(14.35)	(12.76)
3	−0.17(2)	−24.55(14)	−0.03	(−0.35)
4	−0.06(3)	−8.81(19)	0.02	−0.07
5	−0.04(3)	−3.65(17)	0.18	0.17
6	−0.01(3)	−1.77(15)	−0.00	0.02
7	0.00(2)	−0.93(8)	−0.16	−0.12
	C_3/d^3 (K)		440(3)	433(11)
	$\mu_\infty-\mu_0$ (K)		0.79(14)	0.73(15)

Reentrant ($N=16, \bar{T}=145.0$ K)

Layer	Slope	Measured	Residual (4′–8′)	Residual (two-layer)
4′	−0.10(1)	−17.90(3)	−0.28	0.02
5′	−0.06(1)	−6.93(6)	0.54	−0.09
6′	−0.02(1)	−2.96(6)	0.33	0.10
7′	−0.02(1)	−1.37(7)	−0.10	0.05
8′	−0.01(1)	−0.67(5)	−0.49	−0.07
	C_3/d^3 (K)		893(31)	471(3)
	$\mu_\infty-\mu_0$ (K)		1.90(50)	0.78(9)

displayed steps and is associated with an increased slope of the "plateaus" between the steps in the higher-temperature isotherms. The corresponding loci of chemical potential have slightly negative slopes. One possible explanation is to attribute this to substrate heterogeneity: The excess adsorbate is accumulating in regions of stronger binding, perhaps along substrate steps, somewhat in the manner of capillary condensation in powder samples, although not segregated on a large scale compared to the laser wavelength. No hysteresis is observed in the present case, in contrast to capillary condensation. A more likely explanation is that an increasing coverage in disordered, partially filled layers overlies the level at which (more or less) complete layers are being added at the steps. Then the two-layer model used to fit the chemical potentials can be valid at best only at the low-temperature end of the reentrant region. One might attempt to fit both the chemical potentials and the coverage data with a model involving temperature-dependent partial filling in three layers, but we have not done so.

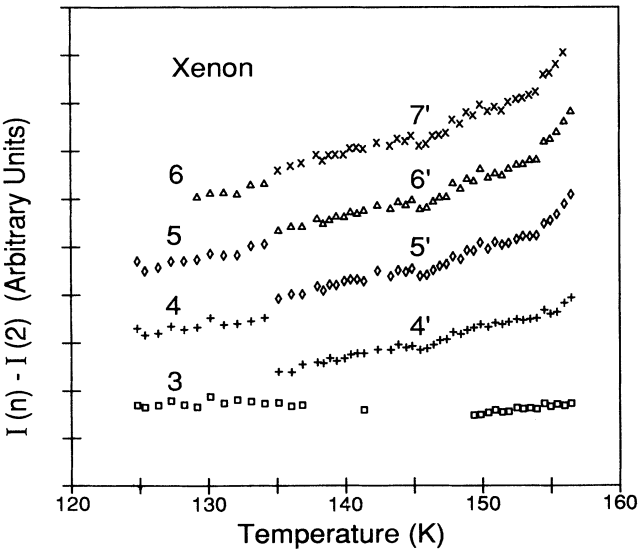

FIG. 7. Ellipsometric coverage at the midpoints of xenon-layer-condensation steps, relative to the midpoint of the second layer, vs temperature.

In most of our isotherms below the bulk melting temperature, the uniform film reaches a maximum coverage equivalent to about 12 layers, and very close to this point there appears strong attenuation of the specular reflection, presumably due to 3D xenon crystallite growth on the graphite. Above the melting point the film grows to about 24 layers. This suggests incomplete wetting of graphite by the solid xenon.

B. Krypton

The phase diagram for submonolayer krypton films on graphite includes a commensurate solid phase, which preempts the liquid-vapor coexistence region. At higher pressures the film has domain-wall fluid and incommensurate solid phases before second-layer condensation.[46] The phase diagram beyond the first layer shows no

reflection of these substantial differences of krypton from xenon or argon in the monolayer region. Volumetric adsorption isotherm studies of krypton on graphite at 77 K by Thomy and Duval[1] showed five sharp steps and continued growth approaching saturation. Transmission electron microscope and RHEED studies found uniform growth of films to ten or more layers at lower temperatures.[11,12] Nham and Hess[32] made an ellipsometric isotherm study covering the range 57–77 K, in which 5–6 layer steps were resolved, and at the higher temperatures attenuation indicated bulk crystallites coexisting with films of 9±1 layers. Volkmann and Knorr[47] measured several ellipsometric isotherms between 55 and 95 K, resolving up to seven steps and directly measuring light scattered by bulk crystallites at a film thickness of 16 layers. In the 95-K isotherm, the third and fourth steps were significantly broadened, in agreement with the results reported below. Larher and Angerand[48] reported layer critical temperatures for layers 2, 3, and 4, based on volumetric measurements. Suter and co-workers[49,50] have made both volumetric and x-ray-diffraction measurements in the region of the second and third layers. They find critical points at $T_{c,2}=98.2$ K and $T_{c,3}=96.2$ K, and they trace a melting transition of the second layer which meets the second-layer condensation line near 93 K and extrapolates to the region of third-layer condensation around 107 K. The x-ray experiments are interpreted as showing that *both* layers of the bilayer become disordered, with the consequence, if true, that $T_{c,2}$ must be a multicritical point, not an Ising critical point. A detailed heat-capacity study in the multilayer regime by Day *et al.*[51] has just been published, and will be discussed below. A study of krypton on a graphite fiber found incomplete wetting below the bulk triple point, with a maximum thickness of four layers at 78 K.[40]

We have conducted two experimental runs with krypton on HOPG. The first, consisting of 48 isotherms over the temperature range 76–116 K, was reported in part in Ref. 42. This run overlaps the high-temperature end of the earlier study of Nham and Hess,[32] which used a different cryostat. The second run produced 77 isotherms between 86 and 116 K. Selected isotherms from the first run are shown in Fig. 8. The evolution is clearly evident (as in the cases of argon and xenon) from stepped isotherms at low temperatures, through layer critical points, then a reentrant region of sharp higher layering transitions, and finally broadening a second time.

For each distinct isotherm step, we measured the pressure and the ellipsometric coverage I_1 at the midpoint of the step, and also the slope at the inflection point of the step. From these we calculate the chemical potential relative to bulk solid-vapor coexistence, the coverage relative to the midpoint of the second layer, and the step width in the chemical potential. The relative coverages for the first krypton run are shown in Fig. 9. As with xenon, step 4′ appears at about 99 K as a small glitch at a coverage corresponding approximately to completion of the third layer, and grows in height and slope with increasing temperature. The higher layers are shifted upward by half a layer or so in the reentrant region relative to the low-temperature region. There is an additional

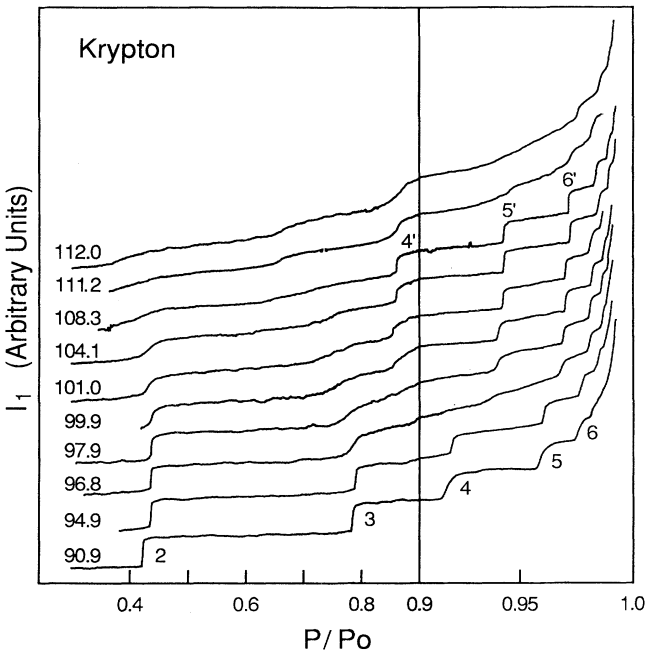

FIG. 8. Selected adsorption isotherms for krypton on graphite, shown as ellipsometric coverage vs reduced pressure. Temperatures are given at the left. The pressure scale is expanded above 0.9.

positive slope of the layer lines at higher temperatures, which is not understood.

The step chemical potentials and step widths for both runs are shown in Fig. 10 by, respectively, the midpoints and the lengths of bars. In the disordering region just above 95 K (e.g., in the 96.8-K isotherm in Fig. 8), in the coverage range of low-temperature step 4, there are two separate rises. For a few isotherms both rises are represented in Fig. 10, where they produce a connection

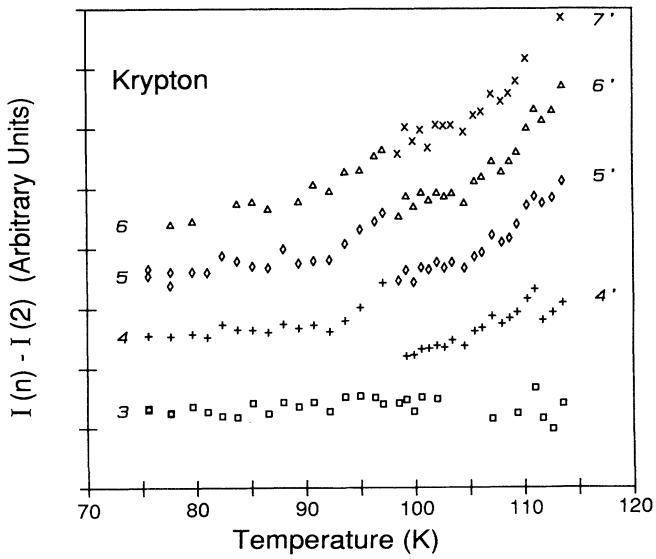

FIG. 9. Ellipsometric coverage at the midpoints of krypton-layer-condensation steps, relative to the midpoint of the second layer, vs temperature.

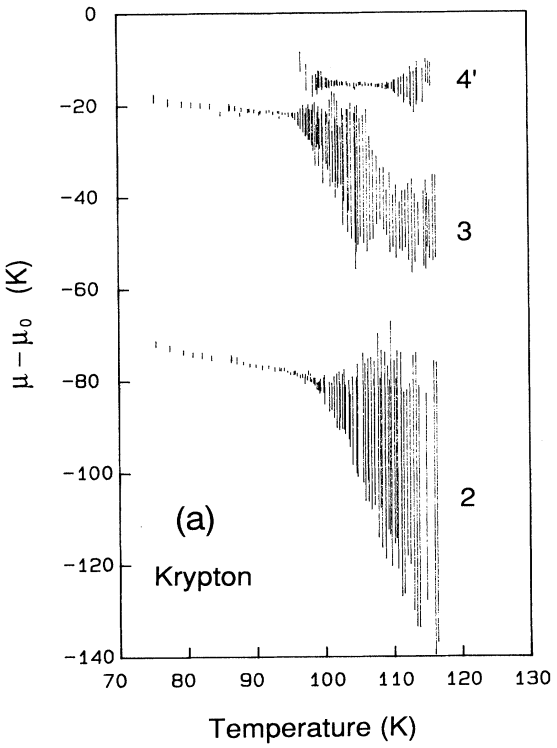

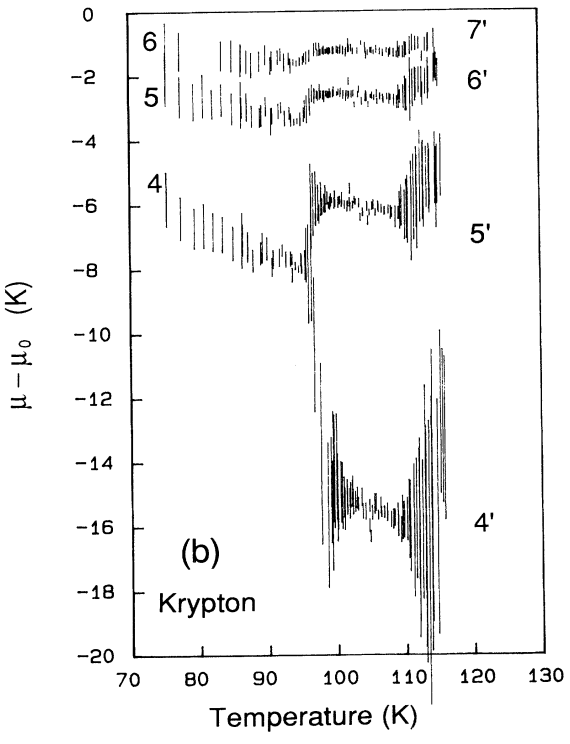

FIG. 10. (a) Krypton-layer-condensation chemical potentials and widths for layers 2, 3, and 4'. (b) Layers 4'–7' on an expanded scale. μ_0 is the chemical potential of the bulk solid-vapor coexistence. Data from both runs are included.

of step 4 to both steps 4' and 5'. The reentrant first-order region is evident in Fig. 10(b). At the highest temperatures, above about 113 K, the chemical potentials of the higher layers again shift upwards, and the step widths appear to decrease slightly, although the steps remain quite broad. This suggests a partial repetition of the process which occurred near 96 K, and may indicate disordering of an additional layer at the surface.

The widths of steps 4', 4-5', and 5-6' as functions of temperature are shown in Fig. 11, with different symbols for the two runs, which are seen to be in excellent agreement. Critical temperatures may be obtained by graphical fits to these data in the regions of departure from the narrowest widths (or from similar graphs of width to the $\frac{4}{7}$ power). The results are given in Table III.

Chemical potentials for layer condensation in the region just below the first critical points were fit with the FHH model described earlier, and the results are summarized in Table IV. Layer chemical potentials in the reentrant first-order region were fit by the modified FHH model, which assumes the top layer is half filled in both coexisting phases, and these fits are also shown in Table IV. The coefficient $C_3/d^3=394$ K-A^3 obtained for the reentrant region is in reasonable agreement with that found for the low-temperature region (365 K-A^3); exact agreement could be obtained by adjusting the assumed top-layer vacancy fraction from 0.50 to about 0.43. The thickness of uniform krypton films at saturation is shown in Fig. 12.

C. Argon

Most experiments indicate that argon forms thick films on graphite at all temperatures which have been studied. RHEED experiments at $T=10$–20 K found uniform growth to at least ten layers,[12] although it is not guaranteed that the adsorbate is in thermodynamic equilibrium or that the chemical potential of the ten-layer

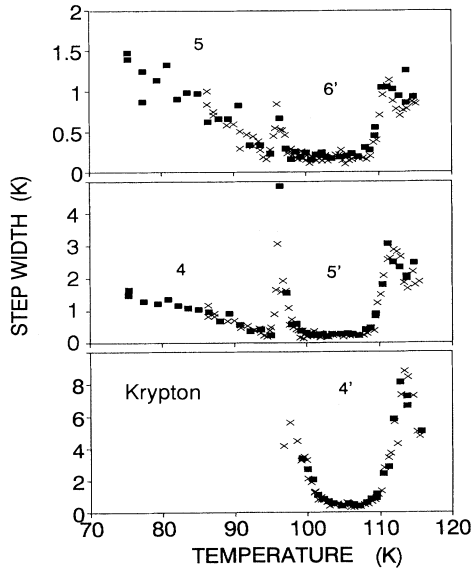

FIG. 11. Widths of several krypton-layer-condensation transitions as functions of temperature. Squares and crosses are data from the first and second runs, respectively.

TABLE III. Krypton-layer critical points, inverse critical points, and second critical points from fits to step widths. The first value is based on the assumptions that $\gamma=\frac{7}{4}$ (Ising critical point) and that the background width adds in quadrature. The value in brackets is based on the assumptions that $\gamma=1$ and that the background width adds algebraically. Mixing these assumptions gives intermediate values. The quoted errors do not include a systematic uncertainty in the temperature scale of up to 0.2 K.

Layer	T_c (K)		Layer	T_i (K)		$T_{c'}$ (K)	
2	97.4(3)	[98.4(3)]					
3	94.9(1)	[95.5(3)]	4′	103.1(5)	[101.6(3)]	108.4(2)	[109.9(2)]
4	95.0(2)	[95.2(2)]	5′	98.8(3)	[98.5(3)]	107.9(2)	[108.9(3)]
5	94.7(3)	[95.1(2)]	6′	98.2(3)	[97.8(3)]	108.2(2)	[108.8(2)]
6	94.9(3)	[95.2(3)]	7′	98.8(8)	[98.3(5)]		[108.8(3)]

film is less than that of bulk solid. Volumetric,[38] and later ellipsometric, isotherms[36,16] near 64 K resolve five or six discrete layers, and show further growth to the equivalent of about 12 layers approaching saturated vapor pressure. Results in conflict with this have been reported for experiments on mass loading of graphite fibers, which found only 4–6 layers at saturation near 61 K.[52]

There have been several detailed studies in the multilayer regime. Zhu and Dash[5] (ZD) made a heat-capacity survey of argon on graphite foam the region between 62 and 90 K and roughly 2–10 statistical layers. Among the features identified were peaks near 68 K associated with the termination of layer coexistence regions; peaks due to melting of individual layers, which for the three layers closest to the substrate could be traced from below to above the bulk melting temperature with increasing total coverage; and large peaks slightly below the bulk melting temperature for coverages exceeding three layers, which are now attributed to melting of capillary condensate. Neutron-diffraction studies of ^{36}Ar multilayers on graphite foam by two groups[53,6,13] have provided information on the lattice constant as a function of thickness at 10 K and, above about 60 K, the prevalence of stacking faults, and the appearance of capillary condensation, which was found to increase rapidly beyond four layers. Layer-by-layer melting of films of several thicknesses was studied by observing the changes in diffraction spectra of the solid film with increasing temperature, and also by measuring the liquid diffraction in a q window on the low-q side of the lowest solid diffraction peak.[6] The results are consistent with the melting loci in the coverage-temperature plane proposed by ZD.

TABLE IV. Layer-condensation chemical potentials and their slopes vs temperature for krypton in a temperature interval below the first critical point, and in the reentrant region (from fits to N isotherms with mean temperature $\bar{T}$). The last two columns give the residuals of fits of Eq. (3) with $d/d_0=0.990$ to the indicated layers, together with the fitting parameters obtained. (Values in parentheses are layers not included in the fit.) The model designated "two-layer" assumes that the top layer is exactly half-filled before and after condensation, so that equal numbers of atoms are added to layers $n=n'$ and $n=n'-1$.

Low T ($N=10, \bar{T}=93.4$ K)

			Chemical potential (K)	
Layer	Slope	Measured	Residual (3–8)	Residual (4–8)
2	−0.20(9)	−77.50(33)	(7.62)	(9.30)
3	−0.10(3)	−21.55(11)	−0.03	(−0.27)
4	−0.06(2)	−7.76(9)	−0.01	−0.06
5	−0.02(3)	−3.29(10)	0.13	0.12
6	0.00(3)	−1.58(8)	0.06	0.07
7	−0.03(5)	−0.79(10)	−0.01	0.01
8		−0.48(9)	−0.16	−0.14
	C_3/d^3		369(2)	365(7)
	$\mu_\infty-\mu_0$		0.55(11)	0.51(12)

Reentrant ($N=9, \bar{T}=106.8$ K)

Layer	Slope	Measured	Residual (4′–8′)	Residual (two-layer)
4′	−0.11(4)	−15.64(12)	−0.19	0.06
5′	−0.05(3)	−6.23(10)	0.34	−0.18
6′	0.01(3)	−2.75(9)	0.23	0.03
7′	−0.01(1)	−1.30(4)	−0.06	0.07
8′	0.00(1)	−0.64(3)	−0.34	0.03
	C_3/d^3		752(21)	394(4)
	$\mu_\infty-\mu_0$		1.48(34)	0.51(12)

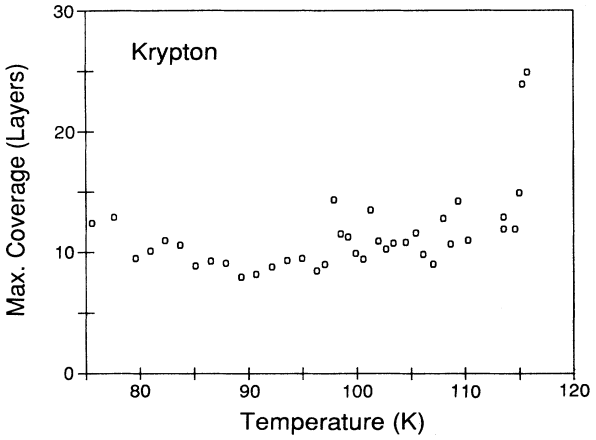

FIG. 12. Krypton film thickness at saturation. A large increase occurs at the bulk melting point, $T_m = 115.76$ K.

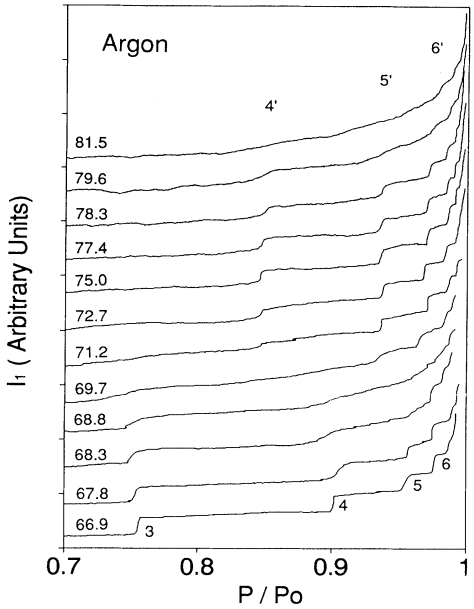

FIG. 13. Selected adsorption isotherms for argon on graphite, shown as ellipsometric coverage vs reduced pressure. Temperatures are given at the left.

Our ellipsometric isotherm study[16,34] found layer critical points near 68 K, in agreement with ZD, but also a reentrant region of first-order layer-condensation transitions at higher temperature, for the fourth and higher layers. In this section we give a more complete report on this work.

Very recently Day, Lysek, LaMadrid, and Goodstein[54] (DLLG) have reported a new heat-capacity study of argon on graphite foam, at coverages from one to six layers after correction for capillary condensation. A vapor pressure isotherm at 77 K on the same substrate shows significant capillary condensation above the fourth, and particularly above the fifth, steps on the ascending branch, and disappearance of the capillary condensate on the descending branch just below the second step. This is in agreement with the neutron-diffraction results. This study provides information on the top-layer disordering process near 67 K, and finds peaks associated with crossing the reentrant coexistence region of three and four layers.

Our study consisted of 68 isotherms between 64 and 82 K, plus isotherms at higher temperatures which do not exhibit discrete steps.[16,34] Figure 13 shows the high-pressure portions of selected isotherms spanning most of the temperature range studied. Second-layer condensation is not shown (off scale to the left). The fourth-layer condensation step becomes extremely broad (68.8-K isotherm) before the appearance of steps 5′ (69.7 K) and 4′ (71.2 K). Steps 5 and 6 have disappeared in the 68.8-K isotherm, and steps 6′ and 7′ are visible at 69.7 K. By 79.6 K the reentrant steps have again become broad.

As before, we calculate the layer-condensation chemical potentials from the step pressures, and we determine the step widths by extrapolating the tangent at the inflection point. Both quantities are presented in Fig. 14, as the centers and lengths of bars, respectively. In this graph, in contrast to Fig. 4(b) for xenon, step 4 appears to evolve continuously into step 4′. This is because we have included the very broad (~ 5 K in chemical potential) fourth-layer condensation in three isotherms near 70 K. Step 4′ proper appears as a small jog in isotherms near 71 K (see Fig. 13), and both steepens and grows in height with increasing temperature until it is almost a full layer step near 75 K. The widths of steps 4–4′, 5′, and 5–6′ are shown in Fig. 15.

In both the low-temperature and reentrant-sharp regions, the layer-condensation lines in Fig. 14 are nearly horizontal, particularly for higher layers. Therefore, according to Eq. (5), the partial entropy in the coverage range spanned by the step must be very nearly equal to the entropy of bulk solid, in both of these regions. In between the partial entropy is larger: The ranges of coverage of steps 4 and 4′ overlap, and isosteres in this overlap range are offset in chemical potential by about -6 K across the roughly 3-K temperature range separating sharp steps 4 and 4′. This implies a partial entropy about $2k_B$ larger than bulk solid, which is comparable to the bulk entropy of melting, $1.7k_B$. Thus when we traverse the region of the fourth layer on an isotherm near 70 K, we are adding coverage with liquidlike entropy. Similar chemical potential offsets are evident in the higher layers, although it is difficult to estimate the slopes of isosteres there. In the low-temperature isotherms, we are adding solid layers at the steps, with presumably only a low density of adatoms (2D gas) on top of the highest solid layer, preceding condensation of the next layer. In the reentrant region, the preceding entropy considerations indicate that we are again adding discrete solid layers at the steps, but now there is a disordered layer, probably liquid, on top of the highest layer. At the low-temperature end of the reentrant region, this disordered layer has coverage equivalent to about 0.5 of a solid layer. This number is suggested both by the direct measure of the ellipsometric coverage relative to the second layer, and by model fits to the chemical potential, discussed below.

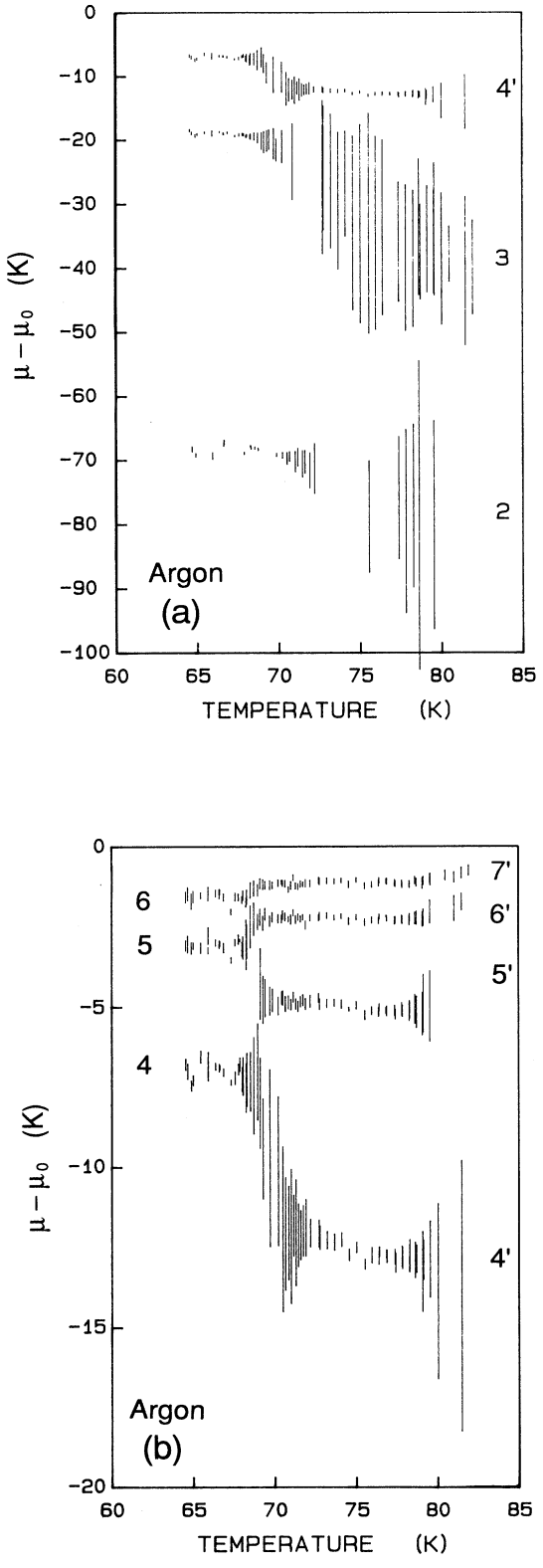

FIG. 14. (a) Argon-layer-condensation chemical potentials and widths for layers 2, 3, and 4'. (b) Layers 4'–7' on an expanded scale. μ_0 is the chemical potential of the bulk solid-vapor coexistence.

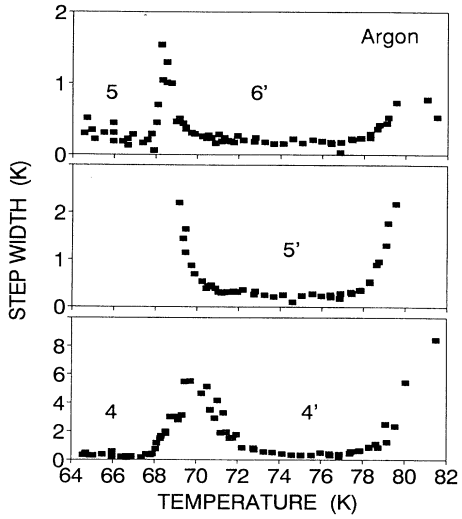

FIG. 15. Widths of several argon-layer-condensation transitions as functions of temperature.

From the step widths we have estimated the layer critical temperatures $T_{c,n}$, as well as the inverse critical temperatures $T_{i,n}$ and second critical temperatures $T_{c,n'}$ bounding the reentrant first-order region. The results are summarized in Table V.

We fit the layer chemical potentials in a temperature interval below the first critical points with the FHH model, as described above. The data and residuals of the fit are given in Table VI. In the reentrant region, chemical potentials of layers 4'–8' were again fit to a modification of the FHH model in which the top layer is assumed to be half-filled; the results are also shown in Table VI. It is noteworthy that essentially the same values for C_3/d^3 are obtained from the two data sets. This implies that, in the context of this model, the best estimate for the vacancy fraction in the top layer is close to 0.50.

At saturation the ellipsometric thickness does not diverge, but, for $T<83$ K, stops at a plateau at the equivalent of 11 ± 1 layers (apart from a small bump near 69 K). The height of the plateau begins to increase just below the bulk melting point, and reaches about 23 layers above the melting point. These data are shown in Fig. 16.

V. DISCUSSION

A. Comparison of adsorbates

An important immediate conclusion is that the adsorption behavior on graphite of the three rare-gas adsorbates studied is nearly identical. If temperature is scaled by the bulk melting temperature (or equivalently, by the bulk critical temperature), chemical potentials are scaled by the fitted value of C_3/d^3, and the ellipsometric coverage signal is scaled by the experimental average step height, then graphs of layer chemical potential versus temperature, step width versus temperature, and midstep coverage versus temperature for the three cases are similar in

TABLE V. Argon-layer critical points, inverse critical points, and second critical points from fits to step widths. The first value is based on the assumptions that $\gamma=\frac{7}{4}$ (Ising critical point) and that the background width adds in quadrature. The value in brackets is based on the assumptions that $\gamma=1$ and that the background width adds algebraically. Mixing these assumptions gives intermediate values. The quoted errors do not include a systematic uncertainty in the temperature scale of up to 0.2 K.

Layer	T_c (K)		Layer	T_i (K)		$T_{c'}$ (K)	
2	69.5(2)	[69.9(2)]					
3	67.7(2)	[68.1(2)]	4′	73.1(4)	[72.0(2)]	77.8(2)	[78.6(2)]
4	67.3(1)	[67.7(1)]	5′	70.7(3)	[69.9(3)]	77.4(2)	[78.1(2)]
5	67.1(1)	[67.8(1)]	6′	70.0(2)	[69.3(2)]	77.2(2)	[78.4(2)]
6	67.6(2)	[68.0(2)]	7′	70.8(3)	[69.5(2)]	76.9(4)	[78.4(3)]

almost every detail. In addition, the limiting coverages of the solid films are similar (12 ± 2, 11 ± 2, and 11 ± 1 layers, respectively, for Xe, Kr, and Ar), and they increase in a similar way at the melting point. There are, however, some systematic departures from this similarity: The reduced first critical temperature (averaging steps 3, 4, 5, and 6) is 0.827 for Xe, 0.820 for Kr, and 0.806 for Ar. Also, in the chemical-potential–temperature plane, the reentrant layers are slightly higher relative to the low-temperature layers for Ar than for Kr or Xe. For Ar the chemical potential of the reentrant layers n' can be modeled as concurrent filling of layers $n-1$ and n in the ratio 0.52:0.48; while for Kr the ratio is 0.43:0.57, and for Xe it is 0.42:0.58.[55]

B. Relation to other recent experiments

Larese and Zhang[56] measured a family of volumetric isotherms for argon on graphite foam between 62 and 75 K and for coverages up to about six layers. These confirm the appearance of step 4′ and show a close similarity to the isotherms in Fig. 13, except for an additional contribution due to capillary condensation. Faul[57] reported measurement of some 20 ellipsometric isotherms for argon on HOPG over the temperature range 40–73 K. From the step widths, he obtained values for $T_{c,2}$ and $T_{c,3}$ which are in close agreement with our values. There is little data at higher coverages above 66 K, so reentrant first-order layering was not observed.

TABLE VI. Layer-condensation chemical potentials and their slopes vs temperature for argon in a temperature interval below the first critical point, and in the reentrant region (from fits to N isotherms with mean temperature $\bar{T}$). The last two columns give the residuals of fits of Eq. (3) with $d/d_0=0..932$ to the indicated layers, together with the fitting parameters obtained. (Values in parentheses are layers not included in the fit.) The model designated "two-layer" assumes that the top layer is exactly half-filled before and after condensation, so that equal numbers of atoms are added to layers $n=n'$ and $n=n'-1$.

Low $T(N=12,\bar{T}=65.8$ K)

		Chemical potential (K)		
Layer	Slope	Measured	Residual (3–7)	Residual (4–7)
2	+0.59(48)	−68.46(35)	(8.64)	(11.36)
3	−0.00(9)	−18.93(6)	0.01	(0.16)
4	0.07(10)	−6.96(7)	−0.07	−0.03
5	0.03(6)	−3.04(4)	0.06	0.07
6	0.05(3)	−1.52(3)	0.04	0.03
7	0.01(6)	−0.87(4)	−0.05	−0.07
	C_3/d^3		314(1)	317(5)
	$\mu_\infty-\mu_0$		0.33(7)	0.36(7)

Reentrant ($N=9,\bar{T}=75.8$ K)

Layer	Slope	Measured	Residual (4′–8′)	Residual (two-layer)
4′	−0.11(7)	−12.70(7)	−0.16	0.04
5′	−0.05(3)	−5.09(3)	0.30	−0.15
6′	0.00(3)	−2.26(2)	0.23	0.06
7′	0.00(3)	−1.13(2)	−0.05	0.06
8′	0.00(2)	−0.65(1)	−0.32	−0.02
	C_3/d^3		592(18)	309(3)
	$\mu_\infty-\mu_0$		1.08(30)	0.30(10)

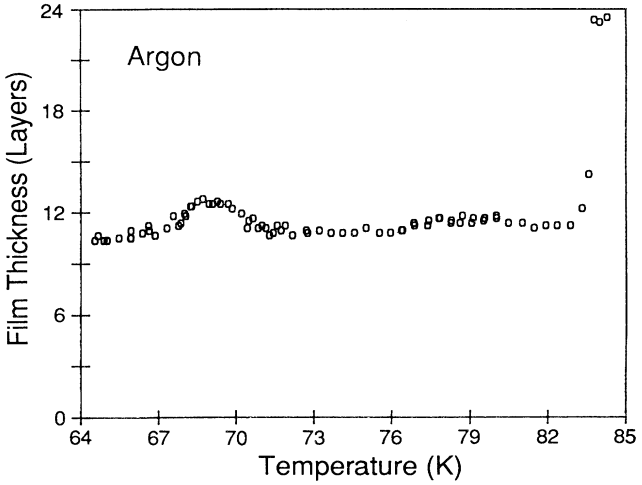

FIG. 16. Argon film thickness at saturation. A large increase occurs at the bulk melting point, $T_m = 83.8$ K.

In our earlier argon paper,[16] we speculated on the basis of partial entropy considerations that there were unseen melting transitions extending from layer $n-1$ near $T_{c,n-1}$ to layer n' near $T_{i,n'}$. Combined with continuous growth of about a half-layer between $T_{i,n'}$ and $T_{c,n}$ this gives a zigzag band of "top-layer melting" near 69 K in the chemical-potential–temperature plane. Subsequently, Gangwar and Suter[49] reported high-resolution volumetric vapor pressure isotherms for krypton on graphite in the range of second- and third-layer condensation, which also showed a weak anomaly attributed to second-layer disordering. This disordering transition intersects the second-layer-condensation line near 93.5 K and extrapolates to the broadened third-layer condensation near 107 K. Hainsey *et al.*[50] also reported x-ray scattering measurements, which confirm disordering of the top layer at this transition, but also led them to conclude that the disorder extends to the first layer, in which case there must be an additional phase transition separating the disordered phase from the ordered monolayer above the second-layer critical point (which is then actually a multicritical point).

Day, Lysek, LaMadrid, and Goodstein[54] (DLLG) have made a detailed heat-capacity study of multilayer argon on graphite foam, considerably extending the earlier work of Zhu and Dash, supplemented by vapor pressure measurements which serve to monitor the chemical potential. They also measured a volumetric isotherm in adsorption and desorption to determine the extent of capillary condensation. Heat-capacity signatures of a large number of phase transitions are identified, many of which can be correlated with our observations. Critical points of the second and third layers are found in close agreement with our critical temperatures. In addition, triple-point melting of the second layer is found 3.7 K below $T_{c,2}$, and in the third layer 1.1 K below $T_{c,3}$, but there is no evidence of triple-point melting in higher layers. Layer coexistence line 4 terminates at 67.5 K, in excellent agreement with our $T_{c,4}$. A line of peaks, presumably due to melting of the third layer, extends from the third-layer triple point to the vicinity of $T_{i,4'}$, and a zigzag line of peaks continues to higher chemical potentials, with vertices near our proposed first critical points and inverse critical points. Peaks on four scans, all at the chemical potential of our step 4′, are identified with leaving the coexistence region 4′. (Scans follow trajectories of decreasing coverage due to desorption.) A line of peaks continues from the high-temperature end of 4′ to well above the bulk melting point, in agreement with ZD, who identified this as the continuation of the third-layer melting line. Peaks are also observed beyond the high-temperature ends of coexistence regions 5′ and 6′.

DLLG point out that the low-temperature coexistence lines 4 and higher may not actually end in critical points. From each of these end points, two lines of heat-capacity peaks extend to higher temperatures, one increasing and the other decreasing in chemical potential. Each of these lines could be a weak first-order phase transition, a higher-order phase transition, or not a thermodynamic phase transition at all. Corresponding to these cases, the end of the layering transition would be a triple point, a multicritical point, or a critical point. For a higher-order transition there should be a change in symmetry; no such change is required on adding an ordered layer beyond the second if it is registered with the rest of the film. Monte Carlo simulations by Phillips[58] and molecular-dynamics simulations by Shrimpton and Phillips[59] indicated that an argon film on graphite will become incommensurate with its lowest layer upon growth to four layers, at least at low temperatures. If this is true in the temperature range of present interest, then there should be a phase transition separating the region of four or more ordered layers from the region of fewer than four ordered layers; however, other levels are unaffected. For brevity, we continue to refer generally to the terminations of layer-coexistence regions as critical points.

Similar considerations apply to the supposed inverse critical points. The triple point in layer 3 suggests that a true phase transition extends to meet the low-temperature end of coexistence region 4′. The slow increase in the height of step 4′ with temperature is quite different from the shapes of the other critical points, and appears more consistent with a multicritical point or a junction with a weak first-order transition. In contrast, the fifth and higher inverse critical points sharpen rapidly to full-layer height, at least roughly as expected for Ising transitions.

Day *et al.*[51] have just reported a detailed heat-capacity study of multilayer krypton films on graphite. The behavior is found to be very similar to argon films, as in our work. One difference is that there is no sign of triple-point melting of the low-temperature third layer, which must, therefore, terminate in a tricritical point or "incipient triple point" rather than a critical point.

Very recently, Larese[60] has completed x-ray-diffraction and QENS measurements on argon on graphite in the neighborhood of the appearance of layer 4′, and Phillips[61] has made detailed Monte Carlo simulations for argon on graphite along five isotherms which span the reentrant region, extending to four-layer coverage. The simulations are validated by good agreement with the experi-

TABLE VII. Comparison of experimental and theoretical values of C_3. All values are in units of meV-Å^3, and experimental values are calculated for assumed layer spacings of 3.63, 3.31, and 3.12 Å for Xe, Kr, and Ar, respectively.

	Experiment		Theory		
Adsorbate	C_3 [Eq. (2)]	C_3 [Eq. (3)]	C_3 (FHH)[a]	C_3 (FHH)[b]	C_3(LPD)[b]
Xenon	1662	1785	1150	1259	1397
Krypton	1097	1141	879	974	1034
Argon	814	830	701	757	784

[a]Based on Rauber *et al.*, Ref. 64.
[b]From Cheng and Cole, Ref. 65.

ments, and should give insight into the mechanism of reentrant layering. In particular, it is found that the 4′ transition at 75 K goes from a state in which the third layer is a lattice fluid with high vacancy density and with substantial population in the fourth and fifth layers, to a state in which the third layer is an ordered solid commensurate with the underlayers, covered by disordered partial fourth and fifth layers.

Alkhafaji and Migone[62] have measured volumetric adsorption isotherms for argon on boron nitride, which has about 21% weaker net adsorption potential than argon/graphite. They report reentrant sharp fourth-layer condensation very similar to argon on graphite, and find in addition that the third layer narrows considerably more at high temperatures than on graphite.

C. FHH model fits

In 1977, Bruch and Watanabe[63] calculated the coefficient C_3 of the polarization energy for krypton and xenon on graphite and, after correcting for the adsorbate-adsorbate attraction, compared to the values obtained by Thomy and Duval[1] (TD) from a single volumetric isotherm for each adsorbate. The agreement was poor: Experimental values were about a factor of 2 larger than theoretical in each case. The values of C_3 which we obtained above are in considerably better agreement with this simplified theory,[64] as can be seen in Table VII. The difference is not primarily in the experimental chemical potentials, which are within 1 K for krypton at 77.3 K, but rather in two differences in the analysis: The value obtained for C_3 is strongly leveraged by the lowest layer included; TD fit the second through the fourth or fifth layers, whereas we start with the third or fourth, on grounds that the potential is not well represented by the asymptotic form for the first few layers. More importantly, TD fit to a potential of the form C_3/n^3d^3, which should be a poorer approximation than Eqs. (2) or (3), especially for the lower layers. We note that Faul[57] actually finds a remarkably good fit to his ellipsometric isotherm for argon at 66 K using this form (with $C_3/d^3=549$ K), even including the first layer; this must be due to a fortuitous cancellation between an inappropriate value of z_0, Eq. (1), and repulsive terms. A fit of Faul's layers 3–7 using Eq. (3) gives a value $C_3/d^3=311$ K, in agreement with our value.

More recently Cheng and Cole[65] have used the theory of Dzyaloshinskii, Lifshitz, and Pitaevski to calculate presumably more accurate values for the coefficient C_3 of the adsorption potential for a number of systems, including the rare gases on graphite. In Table VII, we compare these theoretical values to the experimental values derived above from fits to the layer chemical potentials just below the first critical points. The disagreement is about 23% in the case of xenon, and less for the other gases. The principal uncertainty in this comparison remains the appropriateness of the bulk slab model. Our experimental chemical potentials do not differ greatly from those of TD or Faul.

D. Completeness of wetting

For all three adsorbates we find a limiting film thickness equivalent to 11 or 12 layers at saturated vapor pressure. A possible cause would be a point on the copper sample mount which is colder than the graphite surface, and which therefore clamps the vapor pressure slightly below saturation at the graphite surface. It would require a temperature difference of about 16 mK. Heating by the laser is known to be significantly smaller than this, because attenuation of the laser by a factor of 2 does not shift step pressures measurably. Such a temperature difference conceivably could arise from heat conduction through the vapor from the cell walls (which is shunted by the copper cap). This explanation is unlikely, because we regularly see an onset of attenuation of the laser reflection at the point we identify as saturation, which we attribute to the appearance of bulk crystallites on the graphite in coexistence with the 11–12-layer film. An independent indication of incomplete wetting comes from extrapolation of the layer-condensation chemical potentials from $n=4,\ldots,7$ to infinity. The fits to Eq. (3) consistently give positive values of $\mu_\infty-\mu_0$ in the range 0.3–0.7 K, which corresponds to eight or ten layers at saturation. Part of this may be due to systematic deviations of V_n from the assumed form (a contribution of order 0.1–0.2 K is plausible from the residuals), to nucleation barriers for starting layers, and to systematic errors in the precise identification of p_0, but it does not appear that these effects can account for the whole offset. The large increase in limiting film thickness at the bulk melting point, which is observed for all three adsorbates, seems to us to be strong evidence against a heating effect and for nonwetting by the solid phase. The limiting thickness of order 24 layers above T_m, on the other hand, could well be a heating effect.

It has been predicted that the maximum equilibrium thickness of solid films should be limited to a few tens of layers as a consequence of strain induced by the substrate attraction.[3,17] However, this limiting thickness should be extremely sensitive to the strength of the attraction,[17] in contrast to the experimental result that the limiting thickness is virtually the same for argon, krypton, and xenon. An alternative model proposed by Dash[19] gives a thickness limit due to substrate heterogeneity. If film crystallites with different orientations nucleate on different substrate grains, then grain boundaries in the film must propagate outward as the film grows, with constant energy cost per layer. At some thickness this will exceed the van der Waals potential of the layer, and further uniform growth will be unfavorable. The grain boundary energy is not known, but it is plausibly not greatly different for the three adsorbates, so that the limiting thicknesses should be similar. If this is the mechanism, then experiments on graphite with larger grains than HOPG should allow greater limiting thicknesses. This also offers a possible way to explain the differences between experiments on HOPG and graphite fibers.[40,52] Measurements on natural graphite are in progress.

E. Mechanism of reentrant layering

A central question is why reentrant first-order layering should occur after the surface layer has become disordered and film growth has been continuous over an interval of temperature. One possibility is that the first set of critical points corresponds to a preroughing transition, so that the reentrant region is a disordered-flat phase of the surface.[22] In this case the layering is due to an attractive interaction between up and down steps, such that the surface layer is locked to 50% coverage. However, for this to occur, there should be a related surface reconstructed phase with 50% coverage in the top layer, and this has been difficult to picture.[22]

This behavior can be rationalized to some degree by taking the point of view that the transition near $0.82T_m$ is disordering of the top layer of the bulk surface, as seen in early simulations,[23] with promotion to the next layer and formation of vacancies, and this disordering is only slightly modified by the presence of the substrate, down to three layers. Disordering of the second-to-top layer does not occur until about $0.9T_m$, so in the intervening temperature interval, growth must proceed by adding complete solid layers under a disordered surface layer. Then the question may be turned around to ask why there is an interval of continuous growth near $0.82\ T_m$. This might be attributed to interaction of the substrate with the free surface, which turns a weak Kosterlitz-Thouless roughening transition of the bulk surface into stronger transitions of discrete layers above the substrate. The details are apparently different in the present systems than in other systems such as neon, methane, or nitrogen on graphite, which are similar but do not exhibit continuous growth followed by reentrant layer growth. The simulations of Phillips should help clarify the detailed mechanism in the case of argon, krypton, and xenon.

Our data suggest that the roughening temperatures are about $0.93T_m$, as the thicker films grow layer by layer up to that temperature. Direct observation by Marayama[10] of the shapes of small krypton and xenon crystals suggested roughening temperatures near $0.80T_m$. The change in crystal shape there is rather subtle. Completely rounded crystals were observed above $0.97T_m$. If Maruyama's interpretation is correct, it may be necessary to reexamine the relation of layering to roughening in this more complicated context.

F. Surface melting

There is strong evidence that the top layer of these films melts near $0.82T_m$. There is suggestive evidence that the next-to-top layer of thicker films melts at the end of the reentrant sharp layering region, near $0.93T_m$. It is difficult to carry this approach further, especially since direct measurements such as neutron scattering[6] and even heat capacity are limited to four to six total layers by capillary condensation. We have found that solid films are limited to about 12 layers on our substrate, apparently due to grain boundary or strain energy, whereas liquid films grow much thicker. Figure 16 shows that the limiting thickness of argon films increases by about three layers a few tenths of a degree below T_m, which may indicate that the added thickness is liquid. Very careful measurements in the immediate neighborhood of the melting point would be required to establish this interpretation.

G. Conclusions

We have reported ellipsometric vapor pressure adsorption isotherm studies of xenon, krypton, and argon films on graphite in the multilayer regime. This technique is particularly useful in mapping layer-coexistence regions. It is complementary to heat-capacity studies, such as recent detailed work by Goodstein's group, which scan in a roughly orthogonal direction and are especially sensitive to melting and structural phase transitions. We found regions of reentrant first-order layering above the previously identified layer critical temperatures for layers above the third, in which the coverage of the coexisting films is initially about a half-integer. From our data we estimate the chemical potentials of the various layer-coexistence regions, the critical temperatures at which they terminate, and the relative coverages. The scaled phase diagrams of the three adsorbates were found to be substantially the same. Wetting is found to be not quite complete, due possibly to substrate nonuniformity. Questions raised as to the mechanism of the reentrant layering may be answered by recent simulations and structural studies.[60]

ACKNOWLEDGMENTS

We have benefitted from discussions with many colleagues, including J. Z. Larese, O. E. Vilches, M. A. La

Madrid, M. H. W. Chan, J. M. Phillips, H. Taub, M. den Nijs, J. G. Dash, R. M. Suter, A. D. Migone, G. Torzo, and U. G. Volkmann. We are indebted to D. M. Li and G. G. Reynolds for assistance in data acquisition and reduction, and to J. Wells, A. C. Munson, F. M. Hess, and especially to C. G. Gemmill for assistance in data analysis and programming. This work was supported by National Science Foundation Grant No. DMR-9004108.

---

*Present address: PAL, POSTECH, P.O. Box 125, Pohang City, Kyoungbuk 790-600, Korea.

†Present address: Department of Electrical Engineering and Computer Science, University of California, Berkeley, CA 94720.

[1]A. Thomy and X. Duval, J. Chim. Phys. **66**, 1966 (1969); **67**, 286 (1970).

[2]S. Dietrich, in *Phase Transitions and Critical Phenomena,* edited by C. Domb and J. L. Lebowitz (Academic, London, 1988), Vol. 12, pp. 1–218.

[3]M. Bienfait *et al.*, Phys. Rev. B **29**, 983 (1984).

[4]J. G. Dash, Contemp. Phys. **30**, 89 (1989).

[5]D. M. Zhu and J. G. Dash, Phys. Rev. Lett. **57**, 2959 (1986); Phys. Rev. B **38**, 11 673 (1988).

[6]J. Z. Larese and Q. M. Zhang, Phys. Rev. Lett. **64**, 922 (1990).

[7]M. Bienfait, P. Zeppenfeld, J. M. Gay, and J. P. Palmari, Surf. Sci. **226**, 327 (1990).

[8]J. D. Weeks, in *Ordering in Strongly Fluctuating Condensed Matter Systems,* edited by T. Riste (Plenum, New York, 1979), p. 293.

[9]J. C. Heyraud and J. J. Metois, Surf. Sci. **128**, 334 (1983).

[10]M. Maruyama, J. Cryst. Growth **89**, 415 (1988); **94**, 757 (1989).

[11]G. L. Price and J. A. Venables, Surf. Sci. **49**, 264 (1975); H. M. Kramer, J. Cryst. Growth **33**, 65 (1976).

[12]J. L. Seguin *et al.*, Phys. Rev. Lett. **51**, 122 (1983); J. A. Venables, J. L. Seguin, J. Suzanne, and M. Bienfait, Surf. Sci. **145**, 345 (1984).

[13]J. M. Gay, J. Suzanne, J. G. Dash, and H. J. Lauter, J. Phys. (Paris) **1**, 1279 (1991).

[14]L. J. Lysek, M. LaMadrid, P. Day, and D. Goodstein, Langmuir **8**, 898 (1992).

[15]Product of Union Carbide Corp.

[16]H. S. Youn and G. B. Hess, Phys. Rev. Lett. **64**, 918 (1990).

[17]F. T. Gittes and M. Schick, Phys. Rev. B **30**, 209 (1984).

[18]In this case, the tendency of a free monolayer to *expand* relative to a bulk solid is not overcome by substrate-induced compression, but there is still a unique condition for zero strain.

[19]J. G. Dash, J. Cryst. Growth **100**, 268 (1990).

[20]M. S. Pettersen, M. J. Lysek, and D. L. Goodstein, Phys. Rev. B **40**, 4938 (1989).

[21]D. A. Huse, Phys. Rev. B **30**, 1371 (1984); M. P. Nightingale, W. F. Saam, and M. Schick, *ibid.* **30**, 3830 (1984).

[22]K. Rommelse and M. den Nijs, Phys. Rev. Lett. **59**, 2578 (1987); M. den Nijs, in *Phase Transitions in Surface Films 2,* edited by H. Taub *et al.* (Plenum, New York, 1991), p. 247.

[23]J. Q. Broughton and G. H. Gilmer, J. Chem. Phys. **79**, 5105 (1983); **79**, 5119 (1983); **84**, 5741 (1986); V. Rosato, G. Ciccotti, and V. Pontikis, Phys. Rev. B **33**, 1860 (1986); S. Valkealahti and R. M. Nieminen, Phys. Scr. **36**, 646 (1987); Y. J. Nikas and C. Ebner, J. Phys. Condens. Matter **1**, 2709 (1989); A. L. Cheng and W. A. Steele, Langmuir **5**, 600 (1989).

[24]H. S. Nham and G. B. Hess, Phys. Rev. B **38**, 5166 (1988).

[25]G. Vidali, G. Ihm, H.-Y. Kim, and M. W. Cole, Surf. Sci. Rep. **12**, 133 (1991).

[26]W. A. Steele, *The Interaction of Gases with Solid Surfaces* (Pergamon, Oxford, 1974), pp. 238–241.

[27]M. S. Pettersen, M. J. Lysek, and D. L. Goodstein, Phys. Rev. B **40**, 4938 (1989); J. Krim and J. G. Dash, Surf. Sci. **162**, 421 (1985).

[28]S. Chung, N. Holter, and M. W. Cole, Phys. Rev. B **31**, 6660 (1985).

[29]CTI-Cryogenics, Model 1020.

[30]MKS Instruments, Inc., Model 122 Baratron.

[31]We used primarily the vapor pressure data of C. W. Leming and G. L. Pollack, Phys. Rev. B **2**, 3323 (1970), which do not differ greatly from other published data in the range of interest.

[32]H. S. Nham and G. B. Hess, Langmuir **5**, 575 (1989).

[33]Hinds Instruments, Inc., Model PEM-80 FS5.

[34]H. S. Youn, Ph.D. thesis, University of Virginia (unpublished).

[35]Pressure gauge outputs were also recorded at higher resolution using the ADC in a PAR model 121 lockin amplifier.

[36]J. W. O. Faul, U. G. Volkmann, and K. Knorr, Surf. Sci. **227**, 390 (1990).

[37]A. Inaba, J. A. Morrison, and J. M. Telfer, Mol. Phys. **62**, 961 (1987).

[38]F. Ser, Y. Larher, and B. Gilquin, Mol. Phys. **67**, 1077 (1989).

[39]H. Hong and R. J. Birgeneau, Z. Phys. B: Condens. Matter **77**, 413 (1989).

[40]G. Zimmerli and M. W. H. Chan, Phys. Rev. B **45**, 9347 (1992).

[41]K. Kern and G. Comsa, in *Chemistry and Physics of Solid Surfaces VII,* edited by R. Vanselow and R. F. Howe (Springer-Verlag, Berlin, 1988), p. 65.

[42]G. B. Hess, in *Phase Transitions in Surface Films 2,* edited by H. Taub *et al.* (Plenum, New York, 1991), p. 357.

[43]H. Mannebach, U. G. Volkmann, J. Faul, and K. Knorr, Phys. Rev. Lett. **67**, 1566 (1991).

[44]W. K. Burton, N. Cabrera, and F. C. Frank, Philos. Trans. R. Soc. London, Ser. A **243**, 299 (1951).

[45]R. E. Ecke, J. G. Dash, and R. D. Puff, Phys. Rev. B **26**, 1288 (1982).

[46]E. D. Specht *et al.*, Z. Phys. B **69**, 347 (1987); D. M. Butler, J. A. Litzinger, and G. A. Stewart, Phys. Rev. Lett. **44**, 466 (1980).

[47]U. G. Volkmann and K. Knorr, Surf. Sci. **221**, 379 (1989).

[48]Y. Larher and F. Angerand, Europhys. Lett. **7**, 447 (1988).

[49]R. Gangwar and R. M. Suter, Phys. Rev. B **42**, 2711 (1990).

[50]R. F. Hainsey, R. Gangwar, J. D. Shindler, and R. M. Suter, Phys. Rev. B **44**, 3365 (1991).

[51]P. Day, M. LaMadrid, M. Lysek, and D. Goodstein, Phys. Rev. B **47**, 7501 (1993).

[52]L. Bruschi, G. Torzo, and M. W. H. Chan, Europhys. Lett. **6**, 541 (1988); L. Bruschi and G. Torzo, in *Phase Transitions in Surface Films* (Ref. 42), p. 425.

[53]J. Z. Larese *et al.*, Phys. Rev. B **40**, 4271 (1989).

[54]P. Day, M. Lysek, M. LaMadrid, and D. Goodstein, Phys. Rev. B **47**, 10 716 (1993).

[55]In Ref. 16 we used a model with two partially filled layers. In this way it was possible to fit both chemical potential and coverage data.
[56]J. Z. Larese (private communication).
[57]J. W. O. Faul, Diplomarbeit, Johannes-Gutenberg-Universität zu Mainz (unpublished).
[58]J. M. Phillips, Phys. Lett. A **147**, 54 (1990); J. M. Phillips and T. R. Story, Phys. Rev. B **42**, 6922 (1990).
[59]J. M. Phillips and N. Shrimpton, Phys. Rev. B **45**, 3730 (1992).
[60]J. M. Phillips and J. Z. Larese, Bull. Am. Phys. Soc. **38**, 748 (1993).
[61]J. M. Phillips, Ref. 61 and (private communication).
[62]M. T. Alkhafaji and A. D. Migone, Phys. Rev. B **45**, 8767 (1992); A. D. Migone, M. T. Alkhafaji, G. Vidali, and M. Karimi, *ibid.* **47**, 6685 (1993).
[63]L. W. Bruch and H. Watanabe, Surf. Sci. **65**, 619 (1977).
[64]A more recent calculation is S. Rauber, J. R. Klein, M. W. Cole, and L. W. Bruch, Surf. Sci. **123**, 173 (1982). Additional calculated values of C_3 may be found in Ref. 25.
[65]E. Cheng and M. W. Cole, Phys. Rev. B **38**, 987 (1988). Note that these authors use C_3 in a more restricted sense, and designate the coefficient of the adsorption potential by γ.